



Poster Abstracts: Clinical MRI—Non-ischemic Acquired Heart Disease

261. The Incidence of Cerebral Embolism After Retrograde Catheterization of the Aortic Valve in Degenerative Aortic Stenosis—A Prospective and Randomized Study in 112 Patients Using Diffusion-Weighted Imaging

Torsten Sommer,¹ Matthias Hackenbroch, MD,¹ Alexandra Schmiedel, MD,¹ Sebastian Flacke, MD,¹ Heyder Omran, MD,² H. Schild.¹ ¹Department of Radiology, University of Bonn, Bonn, Germany, ²Department of Cardiology, University of Bonn, Bonn, Germany.

Introduction: Retrograde catheterization of a stenotic calcified valve for determination of the transvalvular pressure gradient is frequently performed for measurement of the severity of aortic stenosis. Retrospective cohort studies examining clinical endpoints have shown that this procedure is associated with a 1–2% risk of clinically apparent neurologic complications. However, the incidence of clinically silent embolism, i.e. the true frequency of structural ischemic brain damage, is unknown.

Purpose: We performed a prospective and randomized study including diffusion-weighted MR imaging (DWI) to assess the incidence of clinically apparent and silent cerebral embolism in patients with degenerative aortic valve stenosis (AS) undergoing cardiac catheterization with transvalvular catheter passage.

Methods: From April 1997 to December 2001, 152 consecutive patients with known or suspected AS were randomized in a 2:1 relationship to receive cardiac catheterization either with (n = 101) or without passage (n = 51) through the aortic valve. Patients underwent MRI of the brain including DWI (b = 0, 500 and 1000 s/mm², TR = 4000 ms, TE = 120 ms, slice thickness 5 mm, matrix 226 × 256) and neurological assessment both within 48 hours before and after the procedure to assess for embolic events. 32 patients

without AS who underwent coronary angiography and ventriculography served as controls.

Results: 22% (22 out of 101) of patients with AS subjected to retrograde catheterization of the aortic valve manifested new focal diffusion abnormalities consistent with acute cerebral embolic events after the procedure; only three of these patients (3%) had clinically apparent neurological deficits. In contrast, none of patients without passage through the stenotic aortic valve nor any of the controls had any evidence of new cerebral embolism as assessed by MRI (p < 0.01).

Conclusions: The frequency of clinically silent ischemic events after retrograde catheterization through a stenotic aortic valve is much higher than the frequency of clinically apparent stroke, indicating that the risk of structural ischemic brain damage in those patients has been markedly underestimated in the past. Therefore, we suggest that patients should be informed about the procedure-related risk and consideration should be given to limiting retrograde catheterization of the stenotic aortic valve to those patients with suboptimal or unclear echocardiographic findings.

262. Right Ventricular Wall Motion Abnormalities Found in Healthy Individuals Using Cardiac Magnetic Resonance Imaging and a New Segmental Model: Impact for the Diagnosis of Arrhythmogenic Right Ventricular Cardiomyopathy

Burkhard Sievers, Ulrich Franken, Marvin Addo, Asli Bakan, Simon Kirchberg, Hans-Joachim Trappe. *Cardiology and Angiology, University of Bochum, Herne, Germany.*

Aims: To evaluate right ventricular wall motion abnormalities in healthy individuals using a new segmental model for the right ventricle.

Methods and results: 29 healthy individuals (9 female, 20 male, mean age 48.9 ± 15 years) underwent magnetic resonance imaging (1.5 Tesla MRI Sonata, Siemens, Erlangen, Germany) to evaluate cardiac function and identify possible right ventricular wall motion abnormalities. TrueFISP gradient-echo sequences with steady-state free precession were used for image acquisition. Right ventricular wall motion abnormalities were analysed and classified according to a segmental model for the right ventricle. In 27 (93.1%) of the 29 individuals right ventricular wall motion abnormalities were found. Dyskinesia was found in 22 (75.9%), hypokinesia in 11 (37.9%) and bulging in eight individuals (27.6%). The number of diagnosed wall motion abnormalities in the transverse plane (86.2%) was significantly higher compared to those found in the short axis plane (13.8%) or in the horizontal longitudinal plane (41.4%) ($p = 0.000$).

Conclusion: Right ventricular wall abnormalities can be found in healthy individuals. Since these wall abnormalities are a criterion for the diagnosis of arrhythmogenic right ventricular cardiomyopathy, wall motion abnormalities around the insertion of the muscular ligaments of the right ventricle should be excluded to prevent an incorrectly positive diagnosis.

263. Cardiac MRI Detects Mild Left Ventricular Hypertrophy and Increased Systolic Function in Obese Subjects

Lilia M. Sierra-Galan, MD,¹ Andrew E. Arai, MD.²
¹Resonancia Magnética Cardiovascular, Hospital

Español de México, México, D.F., Mexico, ²Laboratory of Cardiac Energetics, National Heart, Lung and Blood Institute/National Institutes of Health, Bethesda, MD, USA.

Introduction: Cardiac MRI is well accepted as a gold standard technique for basic cardiac measurements such as left ventricular volumes and mass. To adjust for variation in body size, many investigators index these measurements to body surface area.

Purpose: Since a sizeable fraction of the population is obese, we studied whether cardiac dimensions and volumes varied with obesity and how well normalization by body surface area adjusted these measurements.

Methods: From a database combining MRI reports from two institutions, 150 studies were qualitatively identified as normal. Patients were divided into three groups according to Quetelet's body mass index: normal (<25), overweight (25–30), and obese (>30). Cardiac MRI was performed in multiple long and short axis views using steady state free precession in 93% of subjects and fast gradient echo cine MRI in the remaining 7%. A physician manually analyzed all images with computer-assisted planimetry. The same protocol was used at each institution.

Results: Of the 150 subjects, 76 (51%) were normal weight, 44 (29%) were overweight, and 30 (20%) were obese according to Quetelet's body mass index. There were more women ($n = 94$) than men ($n = 56$) in the study with the following distribution of normal/overweight/obese subjects for women (52%/26%/22%) and for men (48%/36%/16%). The average age was 41.4 ± 15.9 (11–76) for normal,

Table 1. Comparison of volumetric measurements and indexed measurements.

Volumetric measurements	Normal (n = 76)	Overweight (n = 44)	Obese (n = 30)	Comments
LVED volume (ml)	136 ± 33	$150 \pm 28^*$	$159 \pm 28^{***}$	1
LVES volume (ml)	49 ± 15	52 ± 15	49 ± 15	
LV stroke volume (ml)	87 ± 22	$98 \pm 22^{**}$	$110 \pm 22^{***}$	1
LVED mass (g)	100 ± 34	$114 \pm 28^*$	$134 \pm 39^{***}$	3
LVED volume index (ml/m ²)	80 ± 19	79 ± 13	79 ± 10	
LVES volume index (ml/m ²)	29 ± 9	27 ± 8	$24 \pm 7^{**}$	2
LV stroke volume index (ml/m ²)	51 ± 13	52 ± 10	55 ± 9	
LVED mass index (g/m ²)	60 ± 34	60 ± 12	$66 \pm 16^*$	3
LV ejection fraction (%)	64 ± 6	66 ± 7	$69 \pm 8^{***}$	1

Comments: (1) raw measurements that varied significantly between groups, (2) indexed measurements that varied significantly between groups, (3) raw and indexed measurements that varied significantly between groups.

Abbreviations: L = left, V = ventricular, E = end, D = diastolic, S = systolic.

Statistical comparisons with normal group: * = $p < 0.05$, ** = $p < 0.01$, *** = $p < 0.001$.

46.1 ± 13.5 (12–76) for overweight and 43.2 ± 14.8 (15–72) for obese.

Raw measurements of LVED volume and LV stroke volume varied significantly between groups but were normalized well by body surface area (comment 1, Table 1). However, raw measurement of LVES volume did not vary significantly so “normalization” by body surface area created significant differences between normal and obese subjects (comment 2, Table 1). Both raw and indexed LVED mass varied significantly between groups (comment 3, Table 1). LV ejection fraction, which is generally not indexed, increased significantly in the obese subjects (Table 1).

Conclusions: Cardiac volumes and mass vary between normal, overweight, and obese subjects with qualitatively normal MRI studies. Normalization of volumes and dimensions (data not shown) with body surface area appears appropriate for some parameters but inappropriate for others. Fundamentally, however, global systolic function as measured by ejection fraction or fractional shortening appears increased in obese subjects compared with normal subjects. This may represent a need to recruit a higher inotropic state to maintain adequate cardiac output for the obese subject. This may also explain the mild left ventricular hypertrophy in obese subjects as seen on both raw and indexed measurements.

264. Left Ventricular Dimensions and Systolic Function in Obesity

Dorthe Pedersen,¹ Arne V. Astrup,² Henrik B. W. Larsson,³ Lars Sondergaard.⁴ ¹Danish Research Center of Magnetic Resonance, Hvidovre University Hospital, Copenhagen, Denmark, ²Department of Human Nutrition, RVA University, Copenhagen, Denmark, ³MR Center, St. Olav University Hospital, Trondheim, Norway, ⁴Department of Cardiology, Copenhagen University Hospital, Rigshospitalet, Copenhagen, Denmark.

Introduction: It is well known that obesity is associated with increased cardiovascular morbidity and mortality. The cardiovascular risks include ischaemic heart disease as well as heart failure. Several echocardiographic studies indicate an impaired left ventricular (LV) function and an increased left ventricular myocardial mass in obese subjects without any other known cardiovascular disease.

Purpose: To quantify the impact of obesity on LV dimensions and systolic function measured by MRI in otherwise healthy subjects.

Methods: Forty-eight normotensive, obese subjects without history of cardiovascular disease or diabetes were examined (BMI: mean 36 kg/m^2 (SD 1.77), range 32–40 kg/m^2 , age: mean 40 yr (SD 11), range 20–58 yr, sex: 13 male, 35 female) using a whole-body MRI scanner operating at 1.0 tesla with a phased array chest coil as receiver coil. The images were acquired using an electrocardiogram-triggered, breath-hold, gradient-echo technique with an imaging plane in the true short axis of the left ventricle. The temporal resolution was 55 msec, slice thickness 6 mm, field-of-view of $263 \times 350 \text{ mm}^2$ and matrix size 126×256 . The entire LV was enclosed from basis to apex by a stack of imaging planes without inter-slice gaps. For cardiac analysis, endocardial and epicardial borders were manually detected from end-diastolic (ED) images and endocardial borders were also manually drawn from end-systolic (ES) images. LV mass was calculated as the difference between ED epicardial and endocardial volumes multiplied by a density factor 1.05 g/ml. LV stroke volume (LVSV) was calculated as the difference between LVES volumes (LVESV) and LVED volumes (LVEDV), and LV ejection fraction (LVEF) as LVSV/LVEDV . All data were divided by body surface area (BSA) by the formula: $\text{BSA} = \text{Weight}^{0.425} \times \text{Length}^{0.725} \times 0.007184$ for indexation and compared to normative MRI data from the literature (Lorenz, C.H. et al. J. Cardiovasc. MR 1999; 1: 7–21).

Results: LVmass Index was significantly enlarged in subjects with $\text{BMI} \geq 32 \text{ kg/m}^2$ as compared to non-obese subjects (mean 124 g/m^2 (SD 21) vs mean 87 g/m^2 (SD 12)), ($p < 0.001$) whereas LVEDVI (mean 67 ml/m^2 (SD 10) vs mean 66 ml/m^2 (SD 12)), LVSVI (mean 46 ml/m^2 (SD 7) vs mean 45 ml/m^2 (SD 8)) and

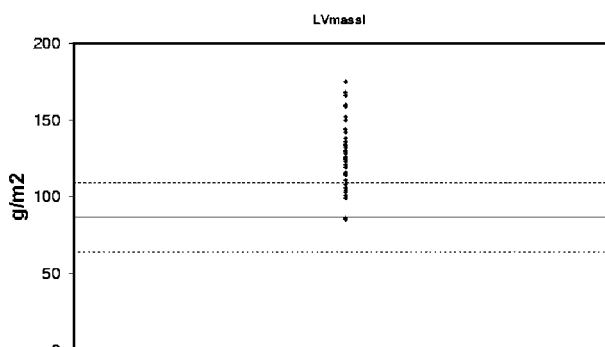


Figure 1. Left ventricular mass/body surface area (g/m^2) in subjects with $\text{BMI} \geq 32 \text{ kg/m}^2$ compared to normative values from the literature (mean: 87 g/m^2 (SD 12)).

LVEF (mean 68% (SD 5) vs mean 67% (SD 5)) were all non-significant. See Figure 1.

Conclusions: Left ventricular mass is significantly increased in obesity, even after correction for BSA. The triggering mechanism behind the hypertrophy is uncertain. However one could speculate increased work load as responsible.

265. Comparison and Normal Values of Three Different Methods for Measurement of Right Sided Cardiac Function

Andreas Kjaer, MD, PhD,¹ Claus L. Petersen, MD, PhD,² Anne-Mette Lebech, MD, PhD,³ Birger Hesse, MD, PhD.¹ ¹Nuclear Medicine, Rigshospitalet, Copenhagen, Denmark, ²Nuclear Medicine, Frederiksberg Hospital, Copenhagen, Denmark, ³Infectious Diseases, Rigshospitalet, Copenhagen, Denmark.

Introduction: Evaluation and monitoring of right sided cardiac function is important in clinical medicine, e.g. in monitoring of patients with primary pulmonary hypertension and before and after lung transplantation. At present, three major methods for measurement of right sided cardiac function exist: cardiac MR, first-pass radionuclide ventriculography (FPRV) as well as equilibrium radionuclide tomographic gated blood pool SPECT (GBPS).

Purpose: To compare and establish normal values of right sided cardiac function using the three most accurate methods currently available.

Methods: Twenty-four healthy volunteers were included. Mean age was 44 years (range: 25–58) and 30% were females. All had normal body mass index (mean: 25 kg/m²; range: 19–32 kg/m²). The volunteers had a cardiac ECG gated MR study performed on a Philips 1.5 T scanner (n = 8) and right ventricular ejection fraction (RVEF) and right ventricular end-diastolic volume index (RVEDVI) calculated with semiautomatic contouring using Philips standard software. FPRV was performed using a bolus of ^{99m}Tc-labelled human serum albumin and a small field-of-view gamma camera (GE Starcam) (n = 24). RVEF was manually calculated by commercially available software (eNTEGRA v. 1.5). FPRV does not allow direct calculation of RVEDVI. GBPS was performed with a dual headed, orbiting gamma camera (GE Millennium) at equilibrium following injection of ^{99m}Tc-labelled human serum albumin (n = 8). RVEF and RVEDVI were semiautomatically calculated using Blood Pool Gated SPECT software (eNTEGRA).

Results: RVEF was 0.59 ± 0.05 (mean ± SD), 0.55 ± 0.05 and 0.54 ± 0.07 when measured by MR, FPRV and GBPS, respectively. No significant differences were found between any of the groups (P > 0.05). RVEDVI was 70 ± 4 (range: 64–76) and 61 ± 17 (range: 44–89) ml/m² when measured by MR and GBPS, respectively. Although no significant difference was found in RVEDVI between the two methods, much larger variability was observed with GBPS compared to MR.

Conclusions: Comparable normal values of RVEF were found using MR, FPRV and GBPS. End-diastolic volumes of the right ventricle were on average similar using MR and GBPS. However, larger variability was observed when using GBPS for measurement of right ventricular end-diastolic volumes, which potentially indicates that MR may be more accurate for this purpose.

266. Early Contrast Enhanced Imaging Improves the Detection of Intraventricular Thrombus

James C. C. Moon, Andrew G. Elkington, Mark Westwood, Anna S. John, Dudley J. Pennell. Royal Brompton Hospital, London, United Kingdom.

Introduction: TrueFISP cine imaging has excellent blood: myocardial delineation and spatial resolution, but the signal intensity of thrombus may be similar to myocardium.

Purpose: To assess whether the use of combined cine and early gadolinium-DTPA CMR offers improved thrombus detection.

Method: Early imaging was performed after bolus (0.1 mmol/Kg) gadolinium-DTPA using a Fixed Long (TI = 400–440 ms) Inversion Recovery Technique (FLIRT) designed to null gadolinium negative tissue. This technique leaves microvascular obstruction and thrombus dark and myocardium/blood pool bright. This technique was developed to demonstrate microvascular obstruction (MVO), but MVO and thrombus share the property of being functionally avascular, excluding gadolinium in the early phase. 16 cases reported as having thrombus were matched (for age, sex, LV function and disease) with 16 cases without thrombus. The patient diagnoses were: 1 failing systemic RV, 1 dilated cardiomyopathy, 2 hypertrophic cardiomyopathy aneurysms, 1 endomyocardial fibrosis, 7 acute and 4 chronic myocardial infarcts. The 32 cases were analyzed in a random order. The observer determined the presence of thrombus initially on the basis of cine imaging alone, and subsequently with both cine and FLIRT imaging.

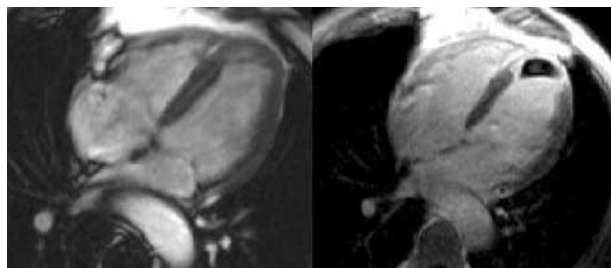


Figure 1. FISP imaging (L) in a patient with an acute MI is inconclusive, but the large thrombus (R) is revealed by early contrast image (R).

The percentage signal difference of thrombus was determined for both techniques.

Results: Using cine imaging alone, 9 (56%) of thrombi were detected with 1(6%) false positive. Using cine and FLIRT, detection improved to 94% with no false positives. Thus cine alone had a sensitivity/specificity of 56% and 93% respectively; cine plus FLIRT 94% and 100%. On cine imaging, where detected, thrombus was 41% darker than blood and 60% brighter than myocardium. Using FLIRT, these improved to 355% ($p = 0.001$) and 133% ($P = NS$), respectively.

Conclusion: The combination of FISP cine imaging with early gadolinium imaging improves the detection of ventricular thrombus over cine imaging alone.

267. Mitral Stenosis Is Accurately Quantified with Velocity-Encoded MRI by the “Pressure Half-Time” Method: Comparison with Doppler Ultrasound

Shiow Juan Lin,¹ Mary P. Watkins,¹ Todd A. Williams,¹ Peggy A. Brown,¹ Katherine A. Lehr,¹ Gregory M. Lanza,¹ Samuel A. Wickline,¹ Shelton D. Caruthers.²
¹Cardiovascular MR Laboratories at Washington University, St Louis, MO, USA, ²Cardiovascular MR Laboratories at Washington University & Philips Medical Systems, Best, Netherlands.

Introduction: Mitral stenosis is a common condition in adults as a consequence of either calcific or rheumatic disease, and requires absolute quantification for appropriate medical and surgical management. Evaluation of mitral valve area noninvasively with Doppler echocardiography provides rapid and accurate analysis of mitral valve disease and serves as a gold standard for clinical medicine. However, the reliability of velocity-encoded Magnetic Resonance Imaging for quantification of mitral valve stenosis has not been defined. Furthermore,

approaches that employ the pressure half-time ($P_{1/2}T$) method for estimating valve size have not been reported. Accordingly, we implemented an MRI phase contrast version of the $P_{1/2}T$ method to estimate the orifice area of stenotic mitral valves and compared these values paired Doppler ultrasound data.

Purpose: The purpose of this study is to define the extent of concordance between mitral valve areas determined by velocity-encoded MRI and Doppler-derived results by analyzing flow velocity data with the $P_{1/2}T$ method in both cases. Furthermore, MR and ultrasound measurements of the maximum velocities across the mitral valve during early and late diastole (E_{max} and A_{max} , respectively) also were compared.

Methods: Twelve sequential patients with an echocardiographic diagnosis of mitral stenosis were recruited. Each patient was imaged using a whole-body MRI unit operating at 1.5 T (Intera CV, Philips Medical Systems, Best, Netherlands). With the use of the velocity-encoded MR technique, quantitative flow images (through-plane encoding) were acquired ($TE/TR/\alpha = 3.0\text{ ms}/6.1\text{ ms}/30^\circ$, Matrix 128×256 , FoV = 350 mm, $thk = 8\text{ mm}$, Temporal Resolution = 30 phases/RR interval). The velocity-encoded MRI series were performed in the left ventricular short axis plane oriented parallel to the mitral valve plane, positioned 1.5 cm from the valve plane toward the apex. The maximum encoding velocity limit (V_{ENC}) was chosen as $\sim 2\text{ m/s}$. If velocity aliasing occurred, the images were re-acquired with a higher V_{ENC} . All MR images were transferred to an offline workstation (EasyVision R5.1, Philips Medical Systems) for quantitative flow analysis. A region of interest was drawn to include the stenotic mitral jet. The peak flow

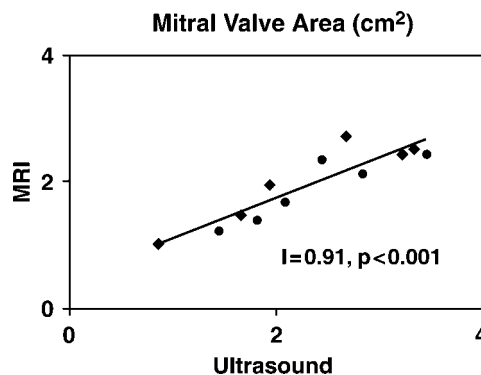


Figure 1. The mitral valve area estimated by the pressure half-time method for both Ultrasound Doppler and velocity-encoded MRI.

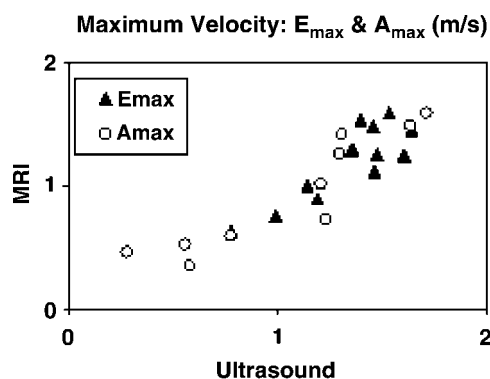


Figure 2. Maximum velocities in early and late diastole, E_{\max} and A_{\max} , respectively, for ultrasound Doppler and velocity-encoded MRI.

velocity through the valve measured in each phase during diastole was used as a starting point to determine the $P_{1/2}T$ by a least squares fitting technique to the linear portion of the flow velocity curves. E and A-wave velocities were defined (E_{\max} and A_{\max}). All MRI values were compared double-blinded with ultrasound measurements, which were recorded by a skilled sonographer and analyzed immediately with the patient remaining on the MRI trolley table. For both MRI and Doppler ultrasound, valve area was estimated as $220/(P_{1/2}T)$.

Results: Figure 1 illustrates excellent concordance between Doppler and MRI valve sizes, suggesting that both $P_{1/2}T$ values and mitral valve areas can be estimated accurately from MRI data ($r = 0.93$ and $r = 0.91$, respectively; $p < 0.001$ each). Figure 2 illustrates the strong correlation between E_{\max} and A_{\max} data for MRI and Doppler ($r = 0.86$ and $r = 0.92$, respectively; $p < 0.001$ each).

Conclusion: Velocity-encoded MRI is a useful and reliable tool for quantification of mitral valve areas with the use of the conventional pressure half-time method. The measurements of the maximum velocities in early and late diastole, and the pressure half-time themselves correlated well with the accepted standard of Doppler ultrasound. These are the first data to our knowledge that illustrate the accuracy of MRI for calculation of mitral valve areas.

268. Myocardial Hyperenhancement in Hypertrophy: Anderson–Fabry Disease Is Different to Hypertrophic Cardiomyopathy

James C. C. Moon,¹ Bhavesh Sachdev,² Andrew G. Elkington,¹ William J. McKenna,² Dudley J. Pennell,¹

Perry M. Elliott.² ¹Royal Brompton Hospital, London, United Kingdom, ²St George's Hospital, London, United Kingdom.

Introduction: Patients with Hypertrophic Cardiomyopathy (HCM) have areas of myocardial hyperenhancement on gadolinium enhanced Cardiovascular Magnetic Resonance (CMR). The cardiac manifestations of Anderson–Fabry disease (AFD) may mimic HCM. AFD is potentially treatable with enzyme replacement therapy and thus diagnosis is important.

Purpose: We hypothesised that gadolinium CMR may be present in AFD and that it could differentiate HCM from myocardial hypertrophy caused by AFD.

Methods: Fifteen male patients (mean 44 ± 12 years) and 7 female heterozygotes (mean 46 ± 12 years) with AFD were compared to 40 patients with familial HCM (28 male, mean 49 ± 17 years). Cine and late gadolinium CMR was performed.

Results: Eight male AFD patients (53%) had myocardial hyperenhancement (mean $7.7 \pm 6.1\%$, range 3.6–20.6%) of total myocardium; percentage hyperenhancement related to LV mass index ($r = 0.79$, $p = 0.0004$) but not to ejection fraction or left ventricular volumes. Hyperenhancement was found in 3 (43%) heterozygous females. In 10 (91%) patients with abnormal gadolinium uptake, hyperenhancement occurred in the mid-myocardial layer of the basal lateral wall (Fig. 1); 2 male patients with severe LVH and systolic impairment had additional hyperenhancement in other myocardial segments. Hyperenhancement in the basal–lateral wall was not seen in the 40 patients with familial HCM.

Conclusions: Individuals with AFD have a unique pattern of myocardial hyperenhancement on CMR that can differentiate them from familial HCM. The reason for this distribution is unknown. Less than 3% of the hypertrophy in AFD is thought due to lipid deposition. These data are in-vivo evidence for focal interstitial expansion in AFD.

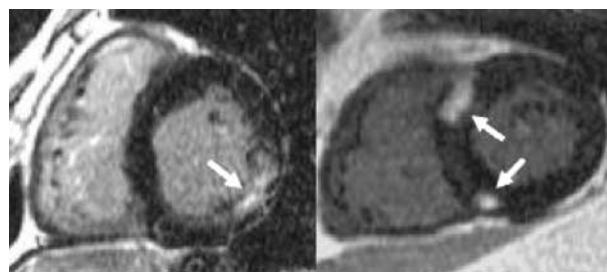


Figure 1. Typical Hyperenhancement in AFD (L) vs a common pattern in HCM (R).

269. Enrasentan Compared with Enalapril in Patients with Asymptomatic Left Ventricular Systolic Dysfunction

Sanjay K. Prasad,¹ Gillian C. Smith, MSc,¹ Henry J. Dargie, MD,² John C. C. Cleland, MD,³ Dudley J. Pennell, MD.¹ ¹CMR Unit, Royal Brompton Hospital, London, United Kingdom, ²Cardiology, Western Infirmary, London, United Kingdom, ³Cardiology, University of Hull, Hull, United Kingdom.

Introduction: Endothelin (ET) is a potent neurohormonal vasoconstrictor. Plasma and myocardial and levels of ET are associated with disease severity in congestive heart-failure and are a powerful predictor of adverse prognosis.

Purpose: In this study, we compared the effect of the orally active dual ET_{A/B} receptor antagonist enrasentan with enalapril on left ventricular (LV) remodeling.

Methods: A multicenter, randomized, double-blind, parallel group study was performed in asymptomatic patients in NYHA 1 with left ventricular dysfunction defined as an LV ejection fraction (EF) $\leq 40\%$ measured by echocardiography or $\leq 45\%$ as measured by cardiovascular magnetic resonance (CMR). Seventy-two patients were randomized to receive either enrasentan (60–90 mg/day, n = 36) or enalapril (10–20 mg/day, n = 36). The primary end-point was the change in LV end-diastolic volume index (LVEDVI) after 6 months treatment as measured by CMR. The secondary objectives were to compare the drug effects on other remodeling and cardiac function parameters; circulating neurohormones; the safety of enrasentan; progression of heart failure; and patient symptoms.

Results: Enrasentan increased LVEDVI ($+3.88 \pm 1.79 \text{ mL/m}^2$) compared with enalapril ($-3.35 \pm 1.39 \text{ mL/m}^2$; $P = 0.001$), and also LV mass index ($+0.67 \pm 1.55 \text{ g/m}^2$ vs $-3.55 \pm 1.6 \text{ g/m}^2$, $P = 0.04$). Enrasentan increased resting cardiac index compared with enalapril ($+0.11 \pm 0.07 \text{ L/m}^2$ vs $-0.096 \pm 0.069 \text{ L/m}^2$; $P = 0.05$). Other remodeling parameters were comparable between groups. Both drugs lowered BNP levels but this was more marked with enalapril (enrasentan $-5.8 \pm 6.9 \text{ pg/mL}$, enalapril $-19.3 \pm 9.4 \text{ pg/mL}$; $P = 0.005$ for the difference). There was no difference in the rate of progression of HF or in the serious adverse event profile.

Conclusions: In asymptomatic patients with LV dysfunction, enrasentan increased LVEDVI compared to enalapril. This would suggest an adverse remodeling effect of enrasentan at a dose of 60–90 mg/day over 6 months, and occurred despite an increase in the resting cardiac index.

270. Right and Left Heart Overload Triggers of Low T3 Syndrome in Patients with Cardiomyopathy: A Magnetic Resonance Study

Michele Emdin, AnnaMaria Sironi, Claudio Passino, Massimo Lombardi. *CNR Institute of Clinical Physiology, Pisa, Italy.*

Introduction: Biologically active thyroid hormone (triiodothyronine, T3), recognizes an inotropic and vasodilator effect, lost in chronic heart failure, when low T3 serum concentrations are frequently observed even in absence of thyroid disease (“euthyroid sick syndrome”).

Purpose: We assessed the hypothesis that the relative contribute of left and right atrial and ventricular overload in heart failure to T3 plasma levels might be different.

Methods: 26 patients (23 males, age 58 ± 2 yrs, body surface area (BSA) $1.92 \pm 0.02 \text{ m}^2$, mean \pm SEM) with idiopathic (15) or postischemic (11) cardiomyopathy underwent cardiac magnetic resonance imaging (MRI) and resting plasma determination of ANP and BNP (IRMA assay, Schering). Left and right atrial and ventricular volumes and function were assessed by MRI (1.5 T, Cvi, GEMS, Milwaukee, USA). A FIESTA sequence was adopted to obtain parallel short axis of the ventricles, and 3D reconstruction was obtained in post-processing.

Results: Left ventricular ejection fraction (LVEF) was 23.7 ± 1.6 , while right ventricular ejection fraction was $29.5 \pm 1.9\%$. End diastolic volumes were 268 ± 18 and $125 \pm 10 \text{ ml}$ for the left and right ventricle, respectively. In the same day blood was sampled at 8 a.m. for thyroid hormones (fT3 and fT4) and TSH in all patients. Plasma fT3 values ranged from 1.33 to 3.17 pg/ml with a mean value of 2.3 ± 0.49 (reference values 2.1–4.2), fT4 was on average $13.2 \pm 2.8 \text{ pg/mL}$ (reference: 7.1–18.5) and TSH $1.63 \pm 0.2 \text{ mUI/ml}$ (reference: 0.3–3.8). Free T3 only (but not fT4 or TSH) positively correlated with either end-diastolic or end-systolic right ventricular volume, ($r = 0.55$, $p = 0.01$ and $r = 0.53$, $P < 0.01$, respectively), and with end-diastolic or end-systolic left ventricular volume, ($r = 0.58$, $p = 0.003$ and $r = 0.60$, $P = 0.002$, respectively). Moreover, a significant negative correlation was observed between fT3 and LVEF ($r = -0.57$, $p = 0.004$).

Conclusions: Decrement in fT3 plasma values is associated with both left/right heart overload and left ventricular dysfunction, possibly explaining the emergent clinical role of low T3 syndrome in heart failure.

Table 1. Patient characteristics.

Age (years sex)	NYHA I–II	NYHA III–IV	CCS I–II	CCS III–IV	Vertigo/Syncope	Previous cardiac decompensation
69 (\pm 9) 27 male	n = 13	n = 21	n = 6	n = 9	n = 7	n = 9

Table 2. Functional CMR measurements.

LVEF (%)	LVEF < 50%	Septal diameter (mm)	AVA (cm ²)	AVA \leq 1.0 cm ²	Bicuspid AV	Concomitant AR
60 \pm 19	n = 13	15 \pm 3	0.77 \pm 0.22	n = 39	n = 17	n = 25

271. Contrast Enhanced CMR Does Not Show Subendocardial Injury in Patients with Severe Aortic Stenosis

Claudio Kupfahl, MD, Marcus Honold, MD, Udo Sechtem, MD, FESC, FACC. *Department of Cardiology, Robert-Bosch-Medical Center, Stuttgart, Germany.*

Introduction: Contrast enhanced magnetic resonance imaging (CMR) using Gd-DTPA can be used for detection of ischemic or inflammatory myocardial injury in different heart diseases. Valvular aortic stenosis (AS) is characterised by left ventricular pressure overload and concentric hypertrophy. This may lead to fibrotic myocardial changes. Furthermore, a previous contrast enhanced CMR study suggested that diffuse ischemic myocardial injury in the subendocardial region occurs regularly in patients with severe AS.

Purpose: We investigated whether fibrotic myocardial changes or ischemic myocardial necrosis and scarring in patients with AS can be visualised using Gd-DTPA contrast enhanced IR-2D FLASH CMR imaging.

Methods: Forty-three consecutive patients with moderate (\leq 1.5 cm²; n = 4) or severe (\leq 1.0 cm²; n = 39) valvular AS were included. Conditions known or suspected to result in delayed Gd-DTPA enhancement such as vascular ischemic events, myocarditis, cardiomyopathies, storage diseases, sarcoidosis and tumours were excluded. Patient characteristics are given in Table 1, functional CMR measurements (True FISP sequences) are shown in Table 2. IR-2D FLASH images (TE 4.38 ms; FA 25°; FoV 340 mm; resolution 1.7 \times 1.3 \times 10 mm; TI 250–350 ms, adjusted individually for optimal nulling of myocardium) were acquired 5 to 20 minutes after injection of 0.1 mmol/kg Gd-DTPA. Data acquisition was performed in short axis views covering the whole ventricle and in standardised long axis views.

Results: Three patients had to be excluded because image quality of IR-FLASH was not sufficient for interpretation due to the fact that patients were not able to hold their breath during measurement or due to suboptimal triggering in cardiac arrhythmias. In 38 patients there was no delayed enhancement detectable. Two patients showed hyperenhancement. The first patient showed localised enhancement extending from the subendocardial layer almost to the epicardium of the midventricular anterior wall. The second patient had focal nontransmural hyperenhancement in the midventricular posterolateral region. Diffuse subendocardial enhancement was not seen in any patient.

Conclusion: In contrast to previous findings, contrast enhanced CMR using IR-2D FLASH does not show diffuse subendocardial enhancement representing ischemic myocardial injury in patients with AS. In addition, CMR using IR-2D FLASH is not able to detect the diffuse fibrosis frequently seen at autopsy in hearts with longstanding pressure overload due to AS. These findings were independent of the severity of AS, hemodynamic status or clinical symptoms of the patients. Localisation and extent of the delayed enhancement seen in the two patients of this study are incompatible with the supposed mechanism of diffuse subendocardial injury caused by reduced myocardial blood flow. It is much more likely that these lesions represent myocardial scar after clinically inapparent myocarditis or coronary embolism.

272. Regional Heterogeneity in 3D Myocardial Shortening in Hypertensive LV Hypertrophy: MR Tagging Substudy to LIFE

Robert W. W. Biederman,¹ Alistair A. Young,² Mark Doyle,¹ Richard B. Devereux,³ Eduardo Kortsik,⁴

Gilbert Perry,⁵ Johnathan N. Bella,³ Suzanne Oparil,⁵ David Calhoun,⁵ Gerald M. Pohost,⁶ Louis J. Dell'Italia, for the LIFE Study Investigators.⁵

¹Allegheny General Hospital, Pittsburgh, PA, USA,

²University of Auckland, Auckland, New Zealand,

³The New York Hospital Cornell Medical Center, New York, NY, USA, ⁴University of New Orleans, New Orleans, LA, USA, ⁵University of Alabama,

Birmingham, AL, USA, ⁶University of Southern California, Los Angeles, CA, USA.

Introduction: High relative wall thickness in hypertensive left ventricular hypertrophy (LVH) has been shown by echocardiography to allow preserved shortening at the endocardium despite depressed LV midwall circumferential shortening (MWCS). A depressed MWCS is an adverse prognostic indicator, but whether this finding is related to global or regional depression of LV myocardial function is unknown, particularly as it relates to 3D myocardial strain patterns.

Methods: Magnetic resonance (MR) tissue tagging permits direct evaluation of 3D intramyocardial strain on a regional basis, independently of LV geometry. We evaluated 21 patients with LVH ECG criteria in the LIFE study and 8 normals, using 3D MR tagging and m-mode echocardiography.

Results: In patients vs. normals, MR LV mass was increased (116 ± 40 vs 63 ± 6 g/m², $p = 0.002$). Neither m-mode fractional shortening (32 ± 6 vs $33 \pm 3\%$) nor mean peak systolic stress were significantly different (175 ± 27 vs 146 ± 28 g/cm²), yet MWCS was decreased by both m-mode (13.42 ± 2.3 vs $18.2 \pm 1.4\%$, $p < 0.001$) and MR (16.8 ± 3.6 vs. $21.6 \pm 3.1\%$, $p < 0.005$). 3D MR MWCS was lower at the base vs. apex ($p = 0.002$) in LVH and greater in lateral and anterior regions vs. septal and posterior regions ($p < 0.001$), contributing to the greater global MWCS estimate by MR. MR longitudinal strain was severely depressed in LVH pts (11.0 ± 3.3 vs $16.5 \pm 2.5\%$, $p < 0.001$) and apical torsion was increased (17.5 ± 4.3 vs $13.7 \pm 3.7\%$, $p < 0.05$). Importantly, both circumferential and longitudinal shortening correlated with the LV wall thickness to radius ratio (h/r) ($r > 0.60$, $p = 0.001$ for both).

Conclusions: In patients with hypertensive LVH, m-mode echocardiography and MRI tagging showed similarly depressed MWCS. However, there was marked intramyocardial heterogeneity in LV myocardial function, leading to an underestimation of global MWCS by echocardiography.

273. The Left Ventricular Outflow Tract Area in Hypertrophic Obstructive Cardiomyopathy Is not Susceptible to Preload Changes—As Assessed by MRI

Jeanette Schulz-Menger, Nidal Al Saadi, Daniel Messroghli, Bernhard Pilz, Rainer Dietz, Matthias G. Friedrich. *Cardiology, Franz-Volhard-Klinik, Charité, Campus Buch, Helios-Klinikum, Berlin, Germany.*

Introduction: In hypertrophic obstructive cardiomyopathy (HOCM), the quantification of the obstruction is an important clinical parameter. The pressure gradient, however, is prone to strong interstudy variations, mainly due to alterations of preload. A planimetry of the left ventricular outflow tract (LVOT) area in images obtained by magnetic resonance imaging (MRI) was shown to be helpful.

Purpose: We hypothesized that the LVOT area itself is less likely to change under different hemodynamic situations than the related pressure gradient.

Methods: We investigated 17 patients with HOCM applying MRI and echocardiography using a repeated protocol for changing the hemodynamic conditions within 2 hours. The LVOT-area was quantified in gradient-echo images (slice thickness 4 mm, TE, TR) acquired with a temporal resolution of less than 35 ms/image in a 1.5 T scanner (Signa CV/I, GE Medical Systems). The pressure gradient was estimated in standard views on a state-of-the-art system (Sequoia 256, Acuson). The protocol included baseline measurements ("native"), measurements after increasing the preload by a 45° elevation of the legs ("45"), and after decreasing the preload by administration of sublingual nitro-glycerin. The latter maneuver was followed by 5 measurements every minute (N1; N2; N3; N4; N5).

The absolute values were quantified and compared to baseline.

Results: The LVOT area was not altered significantly by a change of preload conditions (native: 2.11 ± 0.2 cm²; "45": 2.2 ± 0.2 cm²; N1: 2.0 ± 0.2 cm²; N2: 2.0 ± 0.2 cm²; N3: 1.9 ± 0.2 cm²; N4: 2.0 ± 0.3 cm²; N5: 1.9 ± 0.2 cm²; $p = \text{ns}$). While the Echo-derived pressure gradient did not change significantly by the increase of preload, the application of nitro-glycerin the pressure gradient increased markedly (native: 66 ± 10 mmHg; 45: 64 ± 9 mmHg, $p = \text{n.s.}$; N1: 96 ± 12 mmHg, $p < 0.005$; N2: 93 ± 11 , $p < 0.0005$; N3: 93 ± 12 $p < 0.0001$; N4: 93 ± 14 , $p < 0.005$; N5: 91 ± 14 , $p < 0.0005$).

Conclusions: In addition to its' good correlation to the clinical status, the MRI-derived planimetry of the LVOT area in HOCM is only marginally susceptible

to preload variations. Thus, MRI offers clear advantages over the pressure gradient for the diagnosis and follow-up in patients with HOCM.

274. Myocardial Iron Levels Measured by T2* CMR in Sickle Cell Anaemia

Mark A. Westwood,¹ Lisa J. Anderson,¹ Farrukh T. Shah,² Julian W. Strange,¹ John B. Porter,³ Malcolm J. Walker,³ Dudley J. Pennell.¹ ¹CMR Unit, Royal Brompton Hospital, London, United Kingdom, ²Department of Haematology, University College Hospital, London, United Kingdom, ³Department of Haematology, University College Hospital, London, United Kingdom.

Introduction: Severe sickle cell anemia requires repeated blood transfusions, as does thalassemia major (TM). In TM this leads to myocardial iron accumulation and a dilated cardiomyopathy, causing death in 60%. Cardiomyopathy also occurs in sickle cell anemia, but the aetiology is uncertain. As myocardial iron loading could be a factor in sickle cell cardiomyopathy, we compared the myocardial iron distribution in patients with sickle cell anemia matched for iron loading to those with TM.

Purpose: To assess myocardial iron loading in sickle cell anemia.

Methods: 13 patients with transfusion dependent sickle cell disease (mean age 35 ± 12) were selected, and matched to 13 patients with TM (mean age 22 ± 15) for liver iron loading. Myocardial and liver iron loading were assessed by T2* measurements derived from a gradient echo magnetic resonance sequence. TrueFISP cine images were obtained on all patients for volumetric analysis. Cumulative iron load (from blood bank records) in the sickle group ranged between 0.5–116 g of iron and in the TM patients between 45–275 g.

Results: There was a significant difference ($p < 0.05$) in the myocardial iron load between the sickle cell group (37.0 ± 10.1 ms) as compared to the matched TM group (22.4 ± 15.2 ms). Surprisingly, no patient with a sickle disorder had significant myocardial iron loading, whereas 5 of the TM patients had significant myocardial iron loading ($T2^* < 20$ ms). The mean end diastolic volume was significantly greater in the sickle cell group (187 ± 50 ml vs 143 ± 28 ml, $p < 0.05$), however there was no significant difference in any of the other ventricular function parameters. The liver iron concentrations were well matched, with 5.4 ± 4.9 mg/gdw in

the sickle cell group, and 6.2 ± 5.9 mg/gdw ($p = 0.84$) for the TM group.

Conclusion: Myocardial iron loading does not appear to play a significant role in sickle cell anaemia. The cause for a sickle cell cardiomyopathy remains unclear, and the transfusional iron burden differs significantly between these 2 conditions.

275. Relation Between Gadolinium Hyperenhancement by CMR and Abnormalities on the Surface Electrocardiogram in Hypertrophic Cardiomyopathy

Sanjay K. Prasad, MD,¹ Asifa Quraishi, MBBS,¹ James C. C. Moon, MBBS,¹ Alicia M. Maceira, MD,¹ Perry Elliott, MD,² William J. McKenna, FRCP,² Dudley Pennell, MD.¹ ¹CMR Unit, Royal Brompton Hospital, London, United Kingdom, ²Cardiology, St George's Hospital, London, United Kingdom.

Introduction: Hypertrophic cardiomyopathy (HCM) is a condition with significant morbidity and mortality. It is characterised histologically by myocardial disarray and fibrosis. It is thought that gadolinium hyperenhancement by CMR identifies these fibrotic changes in-vivo, and may be a useful marker for the risk of sudden death. It is also known that ECG abnormalities occur in HCM, including increased PR and QRS duration and abnormal Q waves.

Purpose: We hypothesised that these ECG changes correlated with fibrosis indicated by late gadolinium uptake.

Methods: 39 patients with HCM were studied. The PR interval, QRS duration and the presence of regional Q waves was determined. CMR was performed using a 1.5T Siemens Sonata scanner. Gadolinium hyperenhancement in the myocardium was determined 10–15 minutes after a bolus dose of 0.1 mmol/kg using a standard inversion recovery technique. The mass of hyperenhancement in the left ventricle was assessed using planimetry and related as a percentage of the total left ventricular mass.

Results: 28 (72%) patients demonstrated gadolinium uptake, with the mean percentage of total uptake being 13.9% (SD 10.6%, range 3 to 40%). There was a significant linear correlation between the total percentage of gadolinium uptake and the PR interval ($r = 0.449$; $p = 0.006$), and the QRS duration ($r = 0.38$; $p = 0.017$). However, there was no significant relationship between gadolinium uptake and the presence of Q waves.

Conclusions: Total gadolinium uptake which reflects fibrotic changes correlates with increasing PR interval and QRS duration. These ECG markers could be useful in assessing increased disease severity and risk stratification.

276. Does a 3D Strain Analysis Invalidate 2D Strain Observations in Hypertensive LVH?

Robert W. W. Biederman,¹ Mark Doyle,¹ Alistair A. Young,² Suzanne Oparil,³ Gerald M. Pohost,⁴ Louis J. Dell'Italia, for the LIFE Study Investigators.³ ¹Allegheny General Hospital, Pittsburgh, PA, USA, ²University of Auckland, Auckland, New Zealand, ³University of Alabama, Birmingham, AL, USA, ⁴University of Southern California, Los Angeles, CA, USA.

Introduction: We have previously shown that 2D intramyocardial strain analysis in patients with hypertensive LVH captures heterogeneity that is not present by echocardiography despite preserved LV function. There are many potential non-physiologic reasons that could render such observation erroneous. Yet, there is a compelling morphologic rationale to believe that hypertensive LVH may have disynchronous contractile behavior.

Purpose: We hypothesized that complete 3D intramyocardial strain analysis via MRI radio-frequency tissue tagging may render the MRI derived 2D strain observation invalid in hypertensive LVH patients.

Methods: We evaluated 25 subjects: 17 (10 male) with EKG evidence of LVH criteria in the LIFE study and 8 healthy volunteers (7 male) by 3D MRI tissue tagging using a finite-element modeling approach. Measures of circumferential, radial, longitudinal, as well as maximum principal strain and torsion analysis were performed.

Results: MR derived LV mass was increased in patients as compared to normals (116 ± 40 vs 63 ± 6 g/m², $p = 0.002$) while mean peak end-systolic stress was not significantly different (175 ± 27 vs 146 ± 28 g/cm²) nor was EF (51% vs 55%). Circumferential strain was greater at the apex than at the base ($p = 0.002$) and was greater in the lateral and anterior walls than the septal and posterior walls ($p < 0.001$). 3D longitudinal strain was severely depressed (11.0 ± 3.3 vs $16.5 \pm 2.5\%$ $p < 0.001$), whereas apical torsion was increased compared to normals. The principal 3D midwall contraction strain was also reduced in the patient group tending to become more circumferentially oriented.

Conclusions: A longitudinal gradient was present that allowed for decreased basal circumferential strain

and was mostly offset by markedly increased apical torsional patterns permitting, overall, relatively preserved global function in LVH patients. MRI derived 3D strain by finite-element modeling, not only confirmed the mechanical deformation heterogeneity seen by 2D strain in patients with hypertensive LVH patients, but also demonstrated an order of magnitude increase in such heterogeneity patterns as compared to healthy normals.

277. Evaluation of Time Efficiency of Real Time Navigator Against Breath Hold in Respiratory Compensated Cardiac Exams

Meir Shinnar, MD, PhD,¹ Srirama Swaminathan, PhD.² ¹Medicine/Cardiology, UMDNJ RWJ Medical School, New Brunswick, NJ, USA, ²Philips Medical Systems, Bothell, WA, USA.

Introduction: In cardiac imaging the image quality and the success of the study depends greatly on respiratory compensation technique that is employed. Respiratory navigator sequences have been introduced and used widely, especially in coronary imaging. We therefore investigated the clinical utility of using respiratory navigators during routine morphological cardiac imaging.

Purpose: To evaluate the clinical utility of Navigator based protocols for respiratory compensation, looking both at the image quality and the temporal efficiency.

Methods: Eight consecutive patients with history of Arrhythmogenic Right Ventricular Dysplasia (ARVD) and one patient referred for a cardiac mass were studied. After informed consent, routine clinical imaging was started on a Philips CVMR system (Philips Medical Systems, Nederland, B.V.) equipped with Master gradients (30 mT/m and a slew rate of 150 T/m/s), Vectorcardiogram gating, and a Philips five element synergy cardiac coil.

Back-to-back high resolution Black Blood short axis (HR BB-SA) images with either RNAV or breathhold (BH) respiratory compensation were then obtained. The sequence was cardiac gated dual inversion T1 weighted Turbo Spin Echo (TSE) sequence with a TR of 1 cardiac cycle, TE of 4.6 ms and an acquisition matrix of 205×256 along the phase and frequency encode directions respectively, with a turbo factor of 32, and a field of view (FOV) of 20 cm. As many slices (5 mm thickness and no gap) as needed to cover the heart with were done. The breathhold was typically 5–9 sec, and the navigator used 7 mm navigator window for both gating

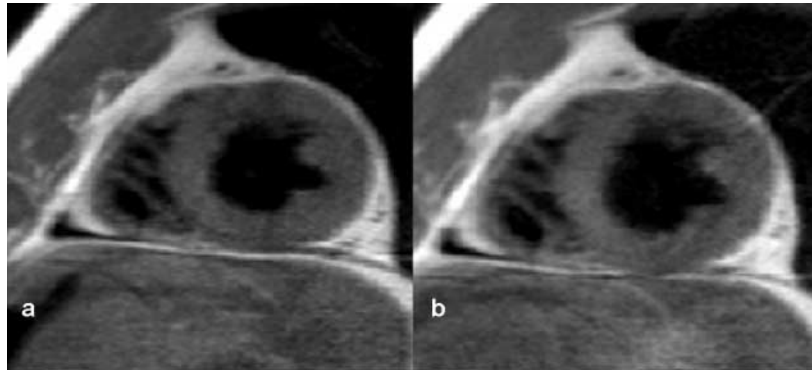


Figure 1. High resolution black blood images a) Breathhold b) Navigator.

and tracking. In some patients, to minimize patient discomfort, the breathhold images were only obtained for the center of the heart.

The images were read independently in a blinded fashion by two physicians. The results were compared with a paired t test.

Results: Representative images from the two protocols are shown in Fig. 1.

Figure 2 shows that the images were judged essentially equal, (two tailed t test p value of 0.6).

The average navigator efficiency was 53%. For breathholding, the average patient required a rest between breathholding at least as long as the breathhold, resulting in a maximal efficiency of 50%, and frequently much lower, especially for longer breathholds.

Conclusions: Navigator respiratory compensation can be easily integrated into routine clinical morphological

imaging, even when high resolution imaging (such as for ARVD) is desired. The image quality is comparable to breathholding. However, it is not limited by patient compliance, and image resolution can be increased. Furthermore, there is no increase in the imaging time required.

278. Can Breathhold Flow Quantification Be Used to Quantify Aortic Stenosis?

Michael Panoutsopoulos, MSc,¹ John P. Ridgway, PhD,² Scott A. Reid, PhD,¹ Mohan U. Sivanathan, MD,² Peter G. Walker, PhD.¹ ¹*School of Mechanical Engineering, University of Leeds, Leeds, United Kingdom,* ²*Cardiac MR, Leeds General Infirmary, Leeds, United Kingdom.*

Introduction: With the introduction of breath hold velocity quantification there is the possibility to perform fast quantification of cardiac function using relatively short echo times. As short echo times are known to be beneficial to the reduction of artefacts and errors in disturbed or turbulent flow, it would seem that breath hold imaging would be a potential candidate for the quantification of valvular stenosis. In particular, aortic stenosis, which is one of the commonest cardiac conditions after coronary disease, is difficult to quantify using current MRI techniques.

Purpose: The purpose of this study, therefore, was to assess the potential for short echo time breath hold imaging in quantifying aortic stenosis.

Methods: All measurements were performed in vitro using a steady flow phantom of aortic stenosis. A water glycerine solution was pumped through a straight Perspex aorta using a steady flow pump. The axi-symmetric aorta, incorporated a sinus section, and allowed the insertion of two axi-symmetric

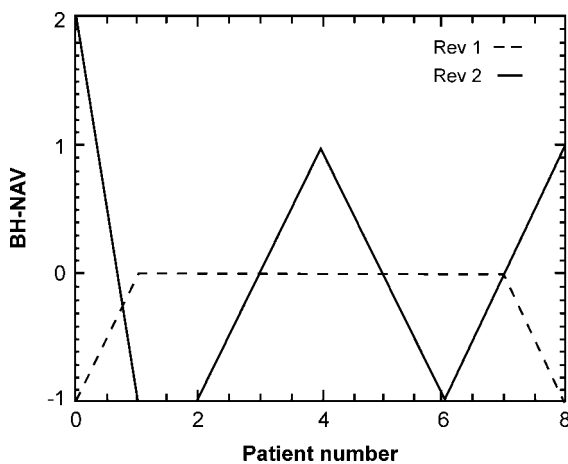


Figure 2. The difference between BH and NAV (positive means NAV was judged better) for the nine patients for the two reviewers.

idealised plastic stenoses of diameters 6 and 10 mm. Flow rates of 20, 15 and 5 l/min were driven through the 10 mm stenosis and those of 6.7, 5 and 3.3 l/min through the 6 mm stenosis. The fluid was doped with gadolinium in order to simulate the T1 and T2 values of blood. Bottles of static fluid were placed around the model.

For the imaging, a Philips 1.5 T ACS-NT MR scanner (Release 6 software) was used utilising their Synergy Cardiac Coil. Using scout images as guides, 7 transverse breath hold flow encoding slices were placed covering the aortic flow at -50, 0, 20, 40, 60, 80 and 130 mm from the stenosis (positive is downstream). Through plane velocity was encoded. MR parameters were: TR = 4.9 ms, TE = 2.8 ms, FOV = 300 mm, Matrix = 128 × 128 (reconstructed 256), slice thickness = 6 mm. The imaging, although of steady flow, was cardiac triggered such that 13 cardiac phases were collected. A long axis image, centred on the lumen, was also obtained to visualize the turbulent jet.

The data was transferred to a PC and analysed using in-house software VENC (p.g.walker@leeds.ac.uk). The velocity images were background corrected by automatically fitting a parabolic surface to the signal from the static fluid bottles surrounding the phantom. A circle of known size, corresponding to the size of the aortic flow phantom lumen, was then placed around the lumen and the flow rate quantified by integration of the velocity of the lumen area. The mean and standard deviation of the flow rate was calculated over the simulated heart cycle. This flow rate was compared to the actual flow rate set during the MR acquisition.

The MR estimation of pressure drop, P, was calculated by using the formula, $p = 4 \cdot U^2$. U, the velocity was obtained by averaging the four central (relative to the aortic lumen) pixels in the velocity encoded images.

The same flow system was also used to quantify the pressure loss due to the stenoses. Pressure taps, flush with the side of the aortic wall, were drilled at a number of positions downstream from the stenosis. One tap was also located upstream. The pressure at each tap was measured by connecting the pressure tap to a manometer. The pressure drop across the stenosis was calculated by subtracting the upstream pressure from the downstream values.

Results: The long axis MR image showed that a turbulent jet, as indicated by regions of signal reduction, was present downstream of the orifices and that the MR slices covered this region. However, there was a central region protruding downstream from the orifice with little or no signal reduction. From knowledge of turbulent jet

flows, this region can be assumed to be the laminar core of the jet. This is a high velocity laminar region where the fluid velocity is constant.

For flow rate, it was found that there was a good agreement between the MR breath hold measurements and the reference values. At the highest flow rate, 20 l/min, the maximum error was around 11%. This is surprising given the probable level of turbulence within the main body of the jet. The effects of turbulence could be seen, however, when the standard deviations of the measurements were examined. These indicated a significant increase in measurement variation within the body of the jet compared to the upstream and far downstream measurements. Consequently, in pulsatile flow, a cardiac output measured in disturbed flow using breath hold imaging may be a reliable measurement but the individual phases may be unreliable.

A good correlation between the direct measurement with the MR calculated stenotic pressure drop was found ($r = 0.99$). However, the MR pressure was on average 1.5 times that of the direct measurement. This indicates a consistent error in the pressure comparison rather than a random, noise driven one. At present, it is unknown whether this consistent error is due to failing in the MR measurement, the direct pressure measurement, the assumptions in the $p = 4 \cdot U^2$ formula or a combination of all three. The authors plan to perform LDV on the model so that the MR central velocity values can be compared with an independent gold standard velocity quantification. This should clarify this error.

Conclusions: Breath hold MR can apparently accurately quantify mean flow in highly turbulent regions. However, individual phase measurements may be less accurate. The standard stenosis quantification formula, $p = 4 \cdot U^2$, does not predict the actual pressure drop in our experimental apparatus. The strength of the correlation between MR and direct pressure measurements, however, would indicate that this problem may be tractable provided the underlying hemodynamics are better understood.

279. Pericardial Effusion or Epicardial Fat? Improved Discrimination with Phase-Sensitive Inversion Recovery MRI

Christopher K. Dyke, MD, Peter Kellman, PhD, Anthony H. Aletras, PhD, Andrew E. Arai, MD. *NHLBI/National Institutes of Health, Bethesda, MD, USA.*

Introduction: Pericardial effusion is a common clinical finding with potentially important implications but is

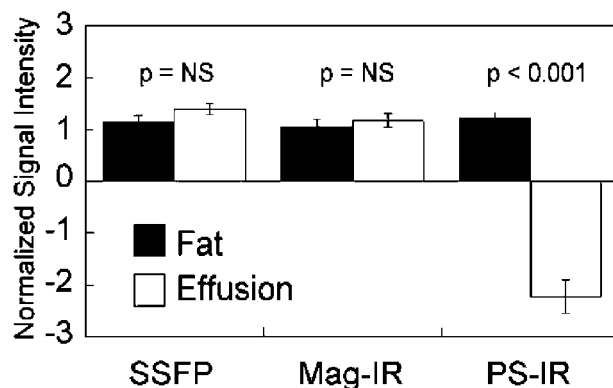


Figure 1.

easily missed using SSFP (FISP) cine and gadolinium enhanced magnitude-reconstructed inversion recovery (Mag-IR) images due to poor contrast vs. epicardial fat despite markedly different T1. Phase-sensitive inversion recovery (PS-IR) has been validated for infarct imaging and has a number of benefits.

Purpose: We proposed that PS-IR would better differentiate pericardial effusion from epicardial fat because PS-IR maintains the polarity of short and long T1 tissues.

Methods: From 392 consecutive patient reports, 53 patients had a pericardial effusion (trace = 28, mild = 14, moderate = 8, severe = 3). The signal intensity of epicardial fat and pericardial effusion was measured in 14 patients imaged with all methods (SSFP, Mag-IR, PS-IR) who had more than a trace effusion.

Results: The signal intensity of fat and effusion were similar using SSFP ($p = \text{NS}$) or Mag-IR ($p = \text{NS}$). Using PS-IR, the fat is bright (positive) but the effusion is dark (negative) ($p < 0.001$).

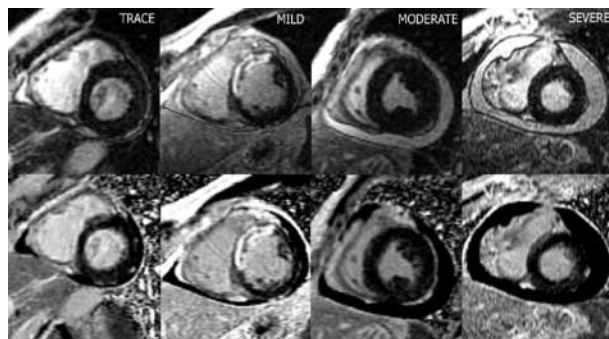


Figure 2.

Figure 2 demonstrates the signal intensity difference between Mag-IR (top row) and PS-IR (bottom row) by varying effusion size. On the Mag-IR images, blood, epicardial fat, and pericardial effusion appear bright. The PS-IR images show a dark pericardial effusion, bright epicardial fat, and dark normal myocardium.

Conclusions: While the most commonly used cardiac MRI parameters have poor contrast between pericardial effusion and epicardial fat, PS-IR reconstruction provides high quality delayed hyperenhancement images and detects effusion without lengthening the typical exam.

280. The Benefit of Aortic Valve Replacement for Aortic Stenosis Is Modulated by CAD

Robert W. W. Biederman,¹ Mark Doyle,¹ June Yamrozik,¹ Jane Ripple,¹ Diane A. Vido,¹ Sunil Mankad,¹ James Magovern,¹ Nathaniel Reichek.²
¹Allegheny General Hospital, Pittsburgh, PA, USA, ²St. Francis Hospital, Roslyn, NY, USA.

Introduction: In patients with severe aortic stenosis (AS), considerable effort has been expended to understand the mechanism of improvement following aortic valve replacement (AVR). While results following AVR have been very encouraging, the actual effects relative to the presence or absence of CAD (CAD +, CAD -) have not been evaluated, yet are important as the population eligible for benefit increases as surgical and medical understanding develops.

Purpose: We hypothesized that the presence of CAD will mitigate the otherwise advantageous effects of reverse remodeling following AVR for AS.

Methods: Eight patients (69–87 yr, 4 female) with severe AS underwent MRI pre AVR and 6.2 ± 1.1 mo post AVR. LV mass indexed to BSA (LVMI) and volume (LVMI/vol) and EF were measured along with 1D transmural circumferential intramyocardial strain (%S).

Results: EF was normal and similar in the two groups at baseline and remained unchanged post AVR (68 ± 12 vs $67 \pm 11\%$, $p = \text{NS}$). However, LVMI (g/m^2) and LVMI/vol ($\text{g}/\text{m}^2/\text{ml}$) were decreased after AVR, indicating that reverse remodeling occurred (95 ± 20 vs $78 \pm 19 \text{ g}/\text{m}^2$, $p < 0.001$ and 0.98 ± 0.30 vs $0.73 \pm 0.20 \text{ g}/\text{m}^2/\text{ml}$, $p < 0.05$, respectively). On sub-set analysis, the fall in LVMI and LVMI/vol were found only in the CAD - patients ($p < 0.05$). Mean %S was higher for the entire group after AVR (23 ± 9 to 25 ± 5 , $p < 0.05$). Notably, however, all

the significance was driven by the marked improvement of %S in the CAD- group (24 ± 9 to $28 \pm 5\%$ following surgery, $p < 0.001$).

Conclusions: Following AVR for AS, there is reverse remodeling, which parallels improvement in intramyocardial function but is not reflected in the calculation of EF. However, despite a perceived population improvement, these benefits are confined to those without CAD. This points towards an altered manner in which the typically favorable post AVR remodeling patterns evolve.

281. Magnetic Resonance Features of Cardiac Carcinoid

Anna S. John, MD, James C. C. Moon, MD, Raad H. Mohiaddin, MD. *CMR Unit, Royal Brompton Hospital, London, United Kingdom.*

Introduction: Carcinoid is a rare tumour (incidence 3.2 per million per year) which produces vasoactive and bronchoconstrictive molecules that can affect the heart if not metabolised first pass by the liver.

Purpose: To characterise the features of cardiac carcinoid by CMR.

Methods: Three patients with cardiac carcinoid underwent CMR on a 1.5T Siemens Sonata scanner. TrueFISP cines of left and right ventricle (LV and RV) and in and outflow tracts were acquired as well as transaxial and sagittal HASTE images to assess cardiac anatomy and the presence of liver metastases. Late enhancement imaging after gadolinium-DTPA (0.1 mmol/kg) was performed using a standard flash inversion recovery sequence. LV and RV volumes, ejection fraction (EF), longitudinal function and right atrial size were measured in 3 patients and 10 healthy controls.

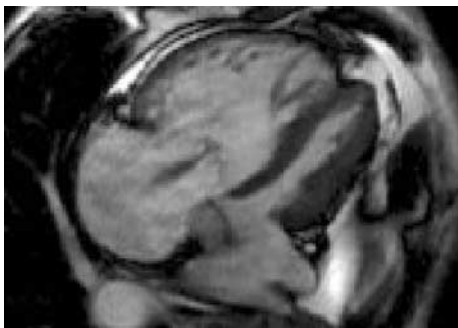
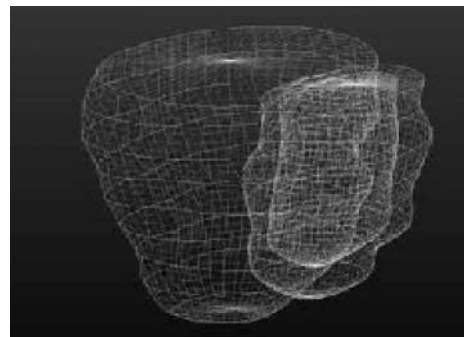


Figure 1. Tricuspid regurgitation and dilated RV.

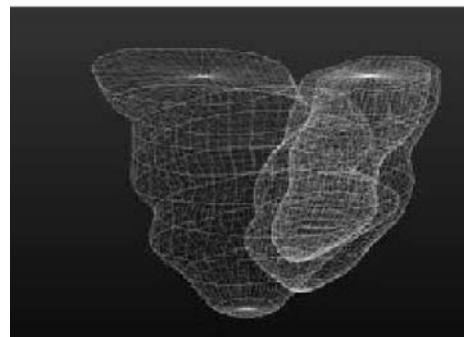


Figure 2. Pulmonary stenosis.

Results: The RV was dilated in all cases, mean EDV 281 ml (range 210–300 ml), ESV 150 ml (101–178 ml). RV long axis function was abnormal in all three (mean percentage change 8.5% versus 24.6%, $p < 0.001$). LV long axis function was unaffected. Mean RV EF was reduced at 46%, LV EF was well within the normal range (mean 62%). Right atrial diameters were enlarged, mean diameter 74×63 mm. The tricuspid valve was severely affected in all cases with thickening and destruction of the leaflets and regurgitation fractions ranging from 45 to



(a)



(b)

Figure 3. Ventricular model in diastole and systole.

62% of RV stroke volumes. The pulmonary valve was affected in all three, two had mixed pulmonary valve disease and one had pulmonary regurgitation only along with signs of pulmonary hypertension. In one patient, right sided endomyocardial fibrosis was detected using inversion recovery late gadolinium imaging. All three showed metastatic infiltration of the liver.

Conclusions: Cardiac carcinoid causes lone right sided disease. CMR is well suited to visualising the pathological appearances which were similar in all cases.

282. A Breath Hold Quantitative Flow Technique for Analyzing Aortic Valve Stenosis: Comparison Between Standard and Segmented K-Space Approaches

Shelton D. Caruthers, PhD,¹ Shioh J. Lin, MSEE,² Mary P. Watkins, RT,² Todd A. Williams, RT,² Katherine A. Lehr, BSN,² Samuel A. Wickline, MD.² ¹Cardiovascular MR Labs, Washington Univ. and Philips Medical Systems, St. Louis, MO, USA, ²Cardiovascular MR Labs, Washington University, St. Louis, MO, USA.

Introduction: The analysis of heart valves can be easily, quickly, and accurately performed using Doppler ultrasound. Specifically, the velocity–time integral (VTI) approach is robust and widely used clinically. Recently, we have shown that velocity-encoded MRI using this same VTI approach is equally robust (1). However, the phase contrast MR technique employed in this analysis was based on an established clinical implementation requiring many minutes of scan time. More current approaches, based on segmented k-space filling, could enable quantitative flow MR imaging within a single breath hold. (2)

Purpose: The purpose of this study was to implement a segmented k-space approach of phase contrast imaging such that all scans required for quantitative flow analysis of the aortic valve could be performed each within a single breath hold. Using the VTI approach for estimating valve size, measurements made with this breath hold technique are compared to the same measurements made with the previously-established non-breath hold technique.

Method: Four patients with aortic valve stenosis were imaged using a 1.5T whole body MRI (Intera CV R8.1.3, Philips Medical Systems, Best, The Netherlands). In addition to standard cine views for qualitative assessment of function, multiple velocity-encoded cine MR images were acquired using both a non-breath hold and a breath hold technique. The non-breath hold

technique ($TE/TR/\alpha = 2.9/5.9/30$, $FoV = 350$ mm, matrix = 128×256 , $thk = 9$ mm, 30 frames/heartbeat) takes about 3.5 minutes (depending on heart rate) for acquiring one imaging slice. The breath hold technique ($TE/TR/\alpha = 2.9/5.9/10$, $FoV = 300$ mm, matrix = 128×256 , with halfscan) is a multi-shot turbo field echo (8 k-lines per segment) typically lasting 20–25 sec with 15–20 frames/heartbeat, depending on heart rate. Both techniques were retrospectively triggered to the vector electrocardiogram. The maximum encoding velocity parameter was chosen such that no flow aliasing occurred in the systolic flow jet (typically about 4 m/s in the aorta, 3 m/s in the LVOT). For each technique, two imaging planes parallel to the aortic valve plane were interrogated—one placed in the ascending aorta 1.5 cm distal to the aortic valve plane, and one in the LVOT at 1.5 cm proximal to the valve plane. Quantitative flow data was analyzed offline (EasyVision R5.1, Philips Medical Systems). To calculate VTI, the area under the curve of the peak flow velocity versus time was summed over systole. From the two imaging planes, Aortic VTI and LVOT VTI were calculated and compared between methods. Functional aortic valve dimension was calculated (using the continuity equation) as the ratio of VTI's multiplied by LVOT cross sectional area. Using the Pearson correlation test, similarity of values from the non-breath hold and breath hold techniques were tested for each of these parameters.

Results: The VTI measurements and functional valve area estimates between breath hold and non-breath hold techniques correlated well. Correlation coefficients between the two methods for VTI's were $r = 0.97$ for the LVOT VTI and $r = 0.99$ for aortic VTI. For pooled

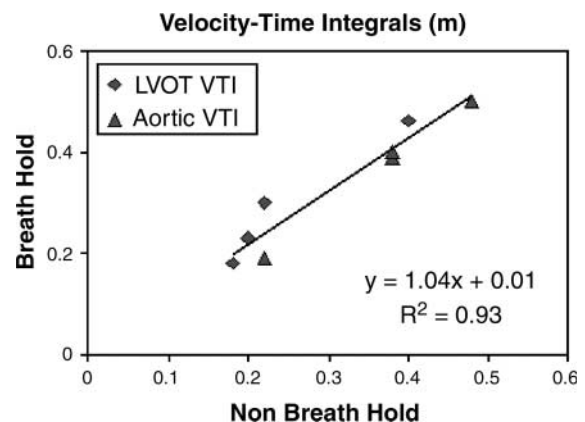


Figure 1. The velocity–time integrals calculated from velocity encoded MR images correlate well between breath hold and non-breath hold techniques.

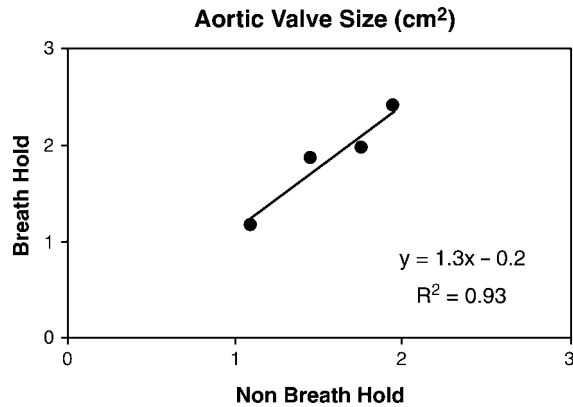


Figure 2. Using the VTI's in the continuity equation approach, functional valves sizes are estimated and correlate well between breath hold and non-breath hold techniques.

VTI's, the correlation coefficient was $r = 0.96$ ($n = 8$) (see Fig. 1). Using the VTI method to estimate the functional valve size, which ranged from 1.1 to 2.4 cm², the two methods agreed with a correlation coefficient of 0.97 (see Fig. 2).

Conclusions: Velocity-encoded MRI can be used as a reliable tool to evaluate flow through stenotic aortic

valves and valve area with VTI measurements.(1) The present results indicate that a segmented k-space approach allows acquisition of all necessary velocity-encoded MR imaging in two short breath holds. Estimates of the valve diameter calculated by the VTI continuity equation method using these data correlate well with previously validated non-breath hold MRI methods. Accordingly, accurate aortic valve size assessments may be greatly accelerated in this approach.

References

1. Caruthers, S.D., Lin, S.J., et al. Comparing velocity-encoded MRI with Doppler ultrasound in the velocity-time integral method of analyzing the aortic valve in patients with aortic stenosis. *J. Cardiovasc. Magn. Res.*, 4:174-5, 2002.
2. Zhang, H., Halliburton, S.S., et al. Ultrafast flow quantification with segmented k-space magnetic resonance phase velocity mapping. *Ann. Biomed. Eng.* 30(1):120-8, 2002.

283. Pulmonary Vein Diameter Measurements Do Not Reflect True Anatomic Variation

Thomas H. Hauser,¹ Susan B. Yeon,¹ Kraig V. Kissinger,¹ Lois Goepfert,¹ Neil M. Rofsky,² Warren

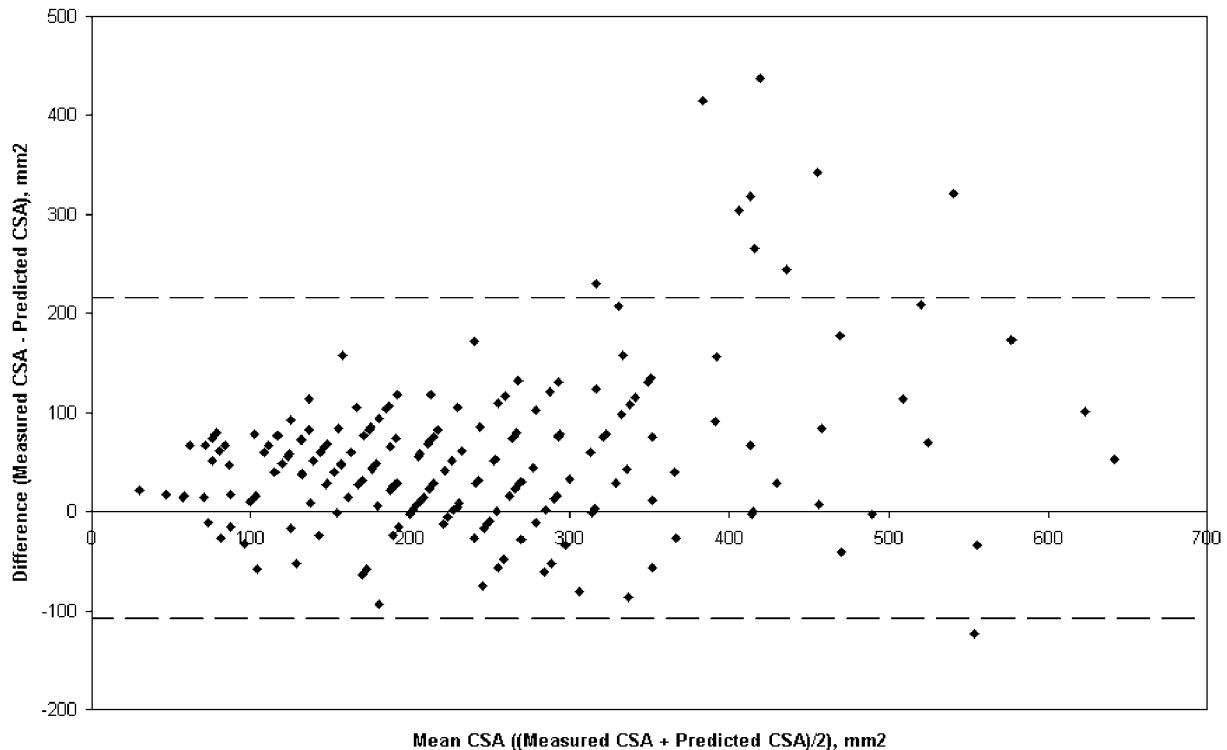


Figure 1. Bland-Altman plot comparing measured and predicted CSA.

J. Manning.³ ¹Medicine, Cardiology Division, Beth Israel Deaconess Medical Center, Boston, MA, USA, ²Radiology, Beth Israel Deaconess Medical Center, Boston, MA, USA, ³Medicine, Cardiology Division, and Radiology, Beth Israel Deaconess Medical Center, Boston, MA, USA.

Introduction: With the advent of radiofrequency ablation of the pulmonary veins (PV) for atrial fibrillation (AF), there has been renewed interest in assessing PV. Magnetic resonance angiography (MRA) visualizes the PVs but there is no standardized method for measuring their size.

Purpose: We evaluated anatomic measurements of the PV with contrast enhanced MRA to determine which measures best reflect true anatomic variation.

Methods: Contrast enhanced MRA of the PVs was obtained in 26 patients with a history of AF prior to planned ablation. The diameter (D) of each vein was measured at its juncture with the left atrium and at its narrowest segment within 5 mm of the juncture. A predicted cross-sectional area (CSA) was calculated as $\pi \cdot (D/2)^2$. The true CSA was then determined from an orthogonal reconstruction of the 3D MRA dataset at the same anatomic positions.

Results: The mean diameter of the PVs was 17.5 ± 4.4 mm at the left atrial juncture and 14.2 ± 4.1 mm at its narrowest segment within 5 mm ($P < 0.001$). The mean CSA was 315 ± 152 mm² at the left atrial juncture and 220 ± 108 mm² at the narrowest segment within 5 mm ($P < 0.001$). The correlation of the D and the predicted CSA to the measured CSA was low (R^2 of 0.65 and 0.66, respectively). A Bland–Altman analysis (see Fig. 1) revealed wide limits of agreement (upper 216 mm², lower -108 mm²)

Conclusion: MRA measurement of both the D and CSA of PVs varies significantly with the orientation and location of measurement, especially with larger diameter veins. The low correlation between both the D and the predicted CSA of PVs with their measured CSA likely results from the non-circular cross-sectional anatomy of the PVs.

284. Value of Segmented TrueFISP Cine MR Angiography in Evaluation of Thoracic Aorta Abnormalities

Olivier Cappellez, MD,¹ Stephane Baldassarre, MD,² Johan Gosset, MD,¹ Jacques Van Espen,¹ Luisa Divano, MD.¹ ¹MRI, CHAMBOR, Mons, Belgium, ²Cardiology, Hôpital Ambroise Paré, Mons, Belgium.

Purpose: To report our experience of segmented TrueFISP pulse sequence in evaluation of disease of the thoracic aorta.

Methods: Between April 2001 and August 2002, 30 patients with thoracic aorta abnormality revealed by echocardiography and/or CT underwent MRI examination that includes at least segmented TrueFISP nonenhanced cine MR angiography and contrast-enhanced 3D MR angiography. 22 aneurysms, 5 postoperative conditions, 2 dissections and 1 aortic ulceration were retrospectively reviewed.

Results: TrueFISP images depict the diagnostic morphologic abnormalities shown by contrast-enhanced 3D MRA in all but one patient where artifacts encroached on the region of interest and compromised the diagnostic information. Nonenhanced cine MR angiography provides supplementary functional information by showing evidence of:

- aortic valvular regurgitation in 13 patients with aneurysm and in 1 postoperative case,
- functional stenosis responsible of mechanical hemolysis in 1 postoperative case
- flow jet at the false lumen entry site in both cases of aortic dissection,
- limited thrombus filling of the aortic ulceration.

Conclusions: In this retrospective review of 30 patients, nonenhanced cine MR angiography was diagnostic for thoracic aorta abnormalities shown on contrast-enhanced 3D MRA in all but one patient. Segmented TrueFISP pulse sequence adds useful functional information to morphologic abnormalities.

285. Characterization of the Myocardial Involvement in Patients with a Systemic Sarcoidosis Applying Contrast-Enhanced Magnetic Resonance Imaging

Jeanette Schulz-Menger, Ralph Wassmuth, Daniel Messroghli, Rainer Dietz, Matthias G. Friedrich. Cardiology, Franz-Volhard-Klinik, Charité, Campus Buch, Helios-Klinikum, Berlin, Germany.

Introduction: The diagnosis of cardiac involvement in proven systemic sarcoidosis is prognostic relevant, but difficult in vivo, which is reflected by conflicting data on the incidence as observed clinically (10%) vs. autopsy-proven cardiac involvement (40%).



Purpose: We investigated the evidence for myocardial inflammation and myocardial fibrosis in cardiac sarcoidosis applying contrast-enhanced MRI.

Methods: We studied 11 patients with proven systemic sarcoidosis and cardiac involvement as defined by the presence of typical symptoms and arrhythmias. The patients were followed during steroid therapy after 6 and 12 months. The data were compared to 1) nineteen patients with proven sarcoidosis but no evidence for myocardial involvement and 2) nine volunteers.

We used standard T1-weighted multislice spin-echo sequences before and after application of 0.1 mmol/kg Gd-DTPA (Magnevist[®], Schering AG; Berlin, Germany) and calculated focal and global relative enhancement (RE). In both groups the delayed contrast accumulation was assessed in T1-weighted gradient echo images 15 minutes after the second bolus of contrast. The left ventricular ejection fraction (LVEF) was calculated using gradient echo sequences.

Results: There was no significant difference in the LVEF between all groups.

RE shows no significant difference between volunteers and patients with sarcoidosis without suspected cardiac involvement.

Both, focal and global RE was significant increased in the patients with suspected cardiac involvement as compared to those without (7.0 ± 1.7 vs. 2.2 ± 0.3 , $p < 0.01$ and 5.9 ± 1.1 vs. 2.4 ± 0.2 , $p < 0.0002$). Follow-up investigations after 6 and 12 months showed a normalization of RE during steroid therapy in 10 of 11 patients.

A delayed enhancement pattern was present only in that patient, in whom the LV function did not improve during steroid therapy.

Conclusions: Contrast-enhanced MRI shows an increased focal and global relative enhancement in patients with sarcoidosis and suspected cardiac involvement, whereas the LVEF remains in a normal range. Delayed enhancement indicating fibrosis was an infrequent finding and was associated with a worse functional outcome.

MRI may be useful for the diagnosis and follow-up of patients with sarcoidosis and suspected cardiac involvement.

286. Late Gadolinium Enhancement in the Cardiomyopathy of Sickle Cell Anemia

Mark A. Westwood,¹ Lisa J. Anderson,¹ Farrukh T. Shah,² John Porter,² Jo Howard,³ Malcolm J. Walker,⁴ Dudley J. Pennell.¹ ¹CMR Unit, Royal Brompton Hospital, London, United Kingdom, ²Department of Haematology, University College Hospital, London, United Kingdom, ³Department of Haematology, Central Middlesex Hospital, London, United Kingdom, ⁴Department of Cardiology, University College Hospital, London, United Kingdom.

Background: One of complications of sickle cell anemia is sickle cell cardiomyopathy. Sickling may lead to small vessel intracoronary thrombosis, the development of sludge infarcts, and hence fibrosis. Magnetic resonance late enhanced gadolinium imaging detects increased extracellular space, the commonest cause in the heart being fibrosis. We therefore looked for areas of myocardial fibrosis in patients with severe sickle cell anemia.

Purpose: To assess for late gadolinium enhancement in severe sickle cell anemia.

Methods: 12 patients with sickle cell anaemia were selected for late gadolinium imaging; all of whom had some evidence of left ventricular dilatation in either systole or diastole. They were given 0.1 mmol/kg of Gadolinium-DPTA intravenously, and late enhancement images were acquired after 10 minutes with a FLASH inversion-recovery sequence, in multiple long and short axis orientations. FISP cine images were obtained for volumetric analysis.

Results: There was no late gadolinium enhancement in the myocardium in any of the patients. The myocardial volumes showed significant ventricular dilatation, but a preserved ejection fraction (Table 1).

Table 1. Left ventricular volumes (normal ranges in brackets).

	End diastolic volume (ml)	End systolic volume (ml)	Ejection fraction	Mass index
Male	196 ± 52 (77–195)	74 ± 35 (19–72)	64 ± 10 (56–87)	114 ± 20 (<113)
Female	170 ± 60 (52–141)	62 ± 45 (13–51)	66 ± 13 (56–87)	86 ± 19 (<95)

Conclusion: Despite evidence of sickle cell cardiomyopathy in these patients, there was no evidence of focal myocardial fibrosis. It therefore seems that either myocardial scarring and infarction does not occur at the microvascular level, or that it is beyond the detection limits of late gadolinium imaging.

287. Delayed Hyperenhancement in Churg–Strauss Syndrome

Ralf Wassmuth, MD, Thomas Poetsch, MD, Ursula Goebel, MD, Friedrich C. Luft, MD, Rainer Dietz, MD, Matthias G. Friedrich, MD. *Franz-Volhard-Clinic, Humboldt University Berlin, Berlin, Germany.*

Introduction: Cardiac disease is known to be the major cause of death in Churg–Strauss syndrome. Magnetic resonance imaging can readily assess various forms of myocardial injuries, however little is known about MRI findings of myocardial involvement in this systemic vasculitis.

Purpose: To test whether MRI can detect myocardial abnormalities in Churg–Strauss syndrome.

Methods: We scanned 7 patients with clinical evidence of Churg–Strauss syndrome that were suspicious for cardiac involvement. Coronary heart disease was ruled out by angiography in 3 of the 7 patients. Left ventricular ejection fraction (LVEF) was quantified with steady state free precession gradient echo imaging. Contrast enhancement was assessed in myocardium and skeletal muscle with multislice T1-weighted spin echo images before and after administration of 0.1 mmol/kg Gd-DTPA. Relative enhancement was calculated as the ratio of myocardial contrast uptake normalized to skeletal muscle and compared to data in 15 normal subjects. After a second dose delayed hyperenhancement images were obtained with inversion recovery gradient echo images.

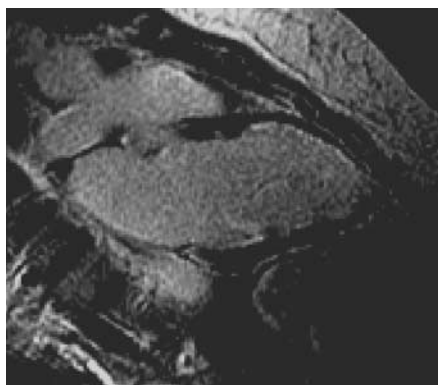


Figure 1.

All patients got at least one follow up study after 3 months.

Results: All patients showed increased relative myocardial enhancement (4.6 ± 1.5) in spin echo imaging compared to controls (2.4 ± 0.5 , $p < 0.03$). Pericardial effusion was present in 3 out of 7 patients. 6 out of 7 patients had transient or permanent deterioration of LVEF below 45%. All of these 6 patients showed evidence of non-transmural, predominantly endocardial, delayed hyperenhancement persisting even after recovery of LVEF. The distribution of the lesions was independent of coronary territories.

Conclusion: Patients with Churg–Strauss syndrome suspicious for cardiac involvement show increased myocardial contrast enhancement. In those with decreased LVEF delayed hyperenhancement can be found, probably representing fibrosis independent of macroscopic coronary disease.

288. Cardiac Dysfunction in HIV Patients

Anne-Mette Lebech, MD, PhD,¹ Andreas Kjaer, MD, PhD,² Claus L. Petersen, MD,³ Jan Gerstoft, MD, PhD,¹ Birger Hesse, MD, PhD.² ¹*Infectious Diseases, Rigshospitalet, Copenhagen, Denmark,* ²*Nuclear Medicine, Rigshospitalet, Copenhagen, Denmark,* ³*Nuclear Medicine, Frederiksberg Hospital, Copenhagen, Denmark.*

Introduction: Cardiac dysfunction is thought to be present in some HIV patients. However, in most cases the dysfunction is sub-clinical. Due to increased survival and antiviral treatment the prevalence of cardiac dysfunction may be increasing. Previous studies have used echocardiography, which is rather imprecise and does not allow for measurement of right-sided cardiac function.

Purpose: To study the prevalence of right and left ventricular dysfunction in a western world HIV population from 2001 to 2002.

Methods: From an outpatient clinic 95 consecutive HIV patients were included. The majority of patients (84%) received highly active antiretroviral treatment (HAART). CD4 cell count was 528 ± 248 cells/mm³ and HIV RNA was fully suppressed in 52% of the patients. All patients had a first-pass radionuclide ventriculography performed in order to estimate right ventricular ejection fraction (RVEF) and a multiple ECG-gated radionuclide equilibrium ventriculography performed in order to establish left ventricular ejection fraction (LVEF). Patients that had a reduced RVEF and/or a reduced LVEF defined as less than 0.50 were asked to

have an additional MR study performed in order to confirm RVEF and LVEF values.

Results: RVEF measured by isotope technique was 0.57 ± 0.07 (range: 0.35–0.74) in the HIV patients. Thirteen (14%) had a RVEF below the normal lower limit of 0.50. Among HIV patients CD4 cell count was 481 ± 203 (range: 75–680) and 534 ± 253 (range: 100–1,300) in the group with reduced RVEF and normal RVEF, respectively ($p > 0.05$). HIV RNA was fully suppressed in 9 of 13 (69%) patients with reduced RVEF and in 36 of 78 (46%) patients with normal RVEF ($p > 0.05$). LVEF measured by isotope technique was 0.60 ± 0.07 (range: 0.47–0.79) in the HIV patients. Three (3%) had a slightly reduced LVEF below the normal lower limit of 0.50. Cardiac MR studies of the patients with reduced RVEF and LVEF are ongoing and will be presented.

Conclusions: In a HIV population where the majority were on HAART a significant part of the patients had a reduced RVEF. However, the reductions in RVEF were only modest.

289. Visualization of Myocardial Edema by Magnetic Resonance Imaging After Septal Artery Embolization in Patients with Hypertrophic Obstructive Cardiomyopathy—Cause for Delayed Improvement

Jeanette Schulz-Menger, Daniel Messroghli, Michael Gross, Rainer Dietz, Matthias G. Friedrich. *Cardiology, Franz-Volhard-Klinik, Charité, Campus Buch, Helios-Klinikum, Berlin, Germany.*

Introduction: Septal artery embolization (SAE) is a therapeutic option in patients with hypertrophic obstructive cardiomyopathy (HOCM). It has been shown, that the desired effect on the obstruction is not completed within the first weeks. However, the underlying cause for this delay is unknown.

Purpose: Magnetic resonance imaging (MRI) visualizes both, the morphological and tissue changes after this intervention.

Methods: We followed 18 patients 44 ± 4 months after SAE with a total of 21 interventions by gradient-echo, T2-weighted (STIR) and contrast-enhanced gradient echo MRI on a dedicated 1.5 T system. The patients were investigated before intervention, and after days 1–3; 7; 14; 28; 90, 180; 360 and then annually. Using gradient echo sequences the left ventricular function and the planimetry of the LVOT-area was quantified. The infarct-related tissue changes were visualized by STIR

for the edema and contrast-enhanced T1-weighted images (delayed enhancement) for the necrosis/fibrosis.

Results: All patients except one (pacemaker implantation 3 y after SAE) were available for follow-up. The LVOT area increased significantly (from 1.3 ± 2 to 2.6 ± 0.2 cm², $p < 0.0001$) during the first three months and remained constant thereafter. In parallel, septal remodeling was completed in the study 3 months after SAE. Whereas the infarct area showed the typical pattern of delayed enhancement throughout the whole observational period, the infarct-related myocardial edema was detectable only during the first four weeks (and thus during remodeling), but not in the subsequent follow-up studies.

Conclusions: Applying Magnetic Resonance Imaging the time course of the infarct-related edema after septal artery embolization can be detected. The changes match that of the increase of LVOT area and thus is likely to be the causative mechanism of the known post-interventional delay of septal remodeling.

290. CMR Findings in Rheumatic Valvular Disease: Initial Experience in Mexico

Aloha Meave, M.D.,¹ Erick Alexanderson, M.D.,¹ Nilda Espinola, M.D.² ¹Magnetic Resonance Unit, National Cardiac Institute, Mexico, D.F., Mexico, ²Echocardiography Unit, National Cardiac Institute, Mexico, D.F., Mexico.

Introduction: Magnetic Resonance is an accurate, reproducible, noninvasive method for optimal assessment of structural and functional parameters in patients with valvular heart disease. Velocity encoded MR imaging can be used to quantify regurgitant blood flow. The severity of valvular stenosis can be determined by evaluating the flow jet and calculating the transvalvular pressure gradient and valve area. Rheumatic fever is the principal cause of valvular heart disease in Mexico.

Purpose: We present our initial experience in patients with rheumatic valvular heart disease comparing the results with those obtained by echocardiography.

Methods: We studied ten consecutive patients with established diagnosis of valvular rheumatic heart disease in a Sonata 1.5T magnet of Siemens with cine gradient-echo MR imaging. We analyzed and quantified the valvular regurgitation detecting the area of signal void jet and calculating the regurgitant fraction. The valvular stenosis was evaluated analyzing the flow jet and the transvalvular pressure gradient and valve area. All

the patients had a previous transthoracic echocardiography study performed few days before the CMR scan.

Results: We found 3 cases of mitral stenosis, 3 with mitral regurgitation, 2 with aortic stenosis and 2 with aortic regurgitation. We obtained ventricular volumetric measurements, anatomic evaluation of the four cardiac chambers and characterization of valve leaflets with CMR technics. The severity degree of valvular stenosis and regurgitation determined by CMR was similar to that obtained by echocardiography. Nevertheless the anatomic characterization of the cardiac structures and the effects of valvular dysfunction with CMR were superior to echocardiography images.

Conclusions: The CMR offers a noninvasive and accurate method for a complete evaluation of patients with rheumatic valvular heart disease. The correlation is similar with echocardiography but offering a better assessment of structural parameters and a more comprehensive evaluation of pathophysiologic changes in this disease.

291. Effect of Oral Sildenafil on Cardiac Function and Remodelling in Patients with Pulmonary Arterial Hypertension

Sanjay K. Prasad,¹ Ghada Mikhail, MD,² Paula Rogers,² Philip Kilner, PhD,¹ Michael Gatzoulis, MD, PhD, FRCP³. ¹CMR Unit, Royal Brompton Hospital, London, United Kingdom, ²Cardiology Unit, Royal Brompton Hospital, London, United Kingdom, ³Adult Congenital Heart Unit, Royal Brompton Hospital, London, United Kingdom.

Introduction: Pulmonary arterial hypertension (PAH) is a progressive disease with a high morbidity and mortality and is associated with right ventricular (RV) dysfunction. Several therapeutic options are available including prostacyclin but are hampered by the mode of administration or expense. Sildenafil promotes vasodilatation in the pulmonary circulation through selective inhibition of phosphodiesterase-type 5 and increased nitric oxide production.

Purpose: Our aim was to determine if oral sildenafil can improve RV function and remodelling as measured by ejection fraction (RVEF), stroke volume, mass and change in RV end diastolic (RVEDV) and RV end systolic volumes (RVESV). We employed cardiovascular magnetic resonance (CMR), to measure these changes.

Methods: Four patients with PAH have been studied thus far (mean age 37 ± 14 yrs; 1 male and 3 females).

Patients underwent initial right heart cardiac catheterisation with vasodilator testing using intravenous sildenafil to ensure no adverse haemodynamic disturbance. They were then commenced on oral sildenafil at 50 mg tds for 3 months. CMR was performed at baseline and after 3 months using a Siemens Sonata 1.5T scanner. All measurements were made by a single blinded experienced operator. In addition, patients underwent a 6 minute walk test.

Results: At 3 months, there was a significant improvement in RV ejection fraction ($29.8 \pm 18.8\%$ to $39.8 \pm 20.4\%$; $P = 0.02$). RVEDV and RVESV both showed a non-significant trend towards reduction. (RVEDV 218.3 ± 82.0 mL to 211.8 ± 93.2 mL, $P = 0.68$; RVESV 158.5 ± 95.9 mL to 146.3 ± 85.1 mL, $P = 0.27$). Left ventricular dimensions and function were unchanged. There was an increase in the 6 min walk test by a mean of 109 metres. Overall, sildenafil was well tolerated by patients but had to be discontinued in 1 patient due to visual disturbance.

Conclusions: Oral sildenafil appears to have a beneficial effect on RV function and remodelling in PAH as determined by CMR. This improvement was associated with increased exercise capacity. Sildenafil may have a role as an adjunct to transplantation.

292. Right Heart Overload Is the Main Trigger of Cardiac Natriuretic Peptides Elevation in Patients with Cardiomyopathy: A Magnetic Resonance Study

AnnaMaria Sironi, Claudio Passino, Concetta Prontera, Massimo Lombardi, Michele Emdin. CNR Institute of Clinical Physiology, Pisa, Italy.

Introduction: Cardiac natriuretic peptides (BNP and ANP), secreted by ventricular and atrial myocytes, respectively, play a key role in volume homeostasis. The plasma concentration of BNP and ANP is raised in heart failure

Purpose: We assessed the hypothesis that the relative contribute of left and right atrial and ventricular overload in heart failure to ANP and BNP plasma levels might be different.

Methods: 26 patients (23 males, age 58 ± 2 yrs, body surface area (BSA) 1.92 ± 0.02 m², mean \pm SEM) with idiopathic (15) or postischemic (11) cardiomyopathy underwent cardiac magnetic resonance imaging (MRI) and resting plasma assay of ANP and BNP (IRMA assay, Schering). Left and right atrial and ventricular volumes and function were assessed by MRI (1.5 T, Cvi, GEMS, Milwaukee, USA). A FIESTA sequence was

adopted to obtain parallel short axis of the ventricles, and 3D reconstruction was obtained in post-processing.

Results: Left ventricular ejection fraction (LVEF) was $23.7 \pm 1.6\%$, while right ventricular ejection fraction was $29.5 \pm 1.9\%$. End diastolic volumes were 268 ± 18 and 125 ± 10 ml for the left and right ventricle, respectively. BNP plasma values ranged from 54 to 783 with a mean value of 241 ± 42 pg/ml, ANP from 36 to 534, mean 134 ± 28 pg/ml. BNP positively correlated with either end-diastolic or end-systolic right ventricular volume, ($r = 0.61$, $p = 0.004$ and $r = 0.74$, $p < 0.001$, respectively), but not with left ventricular volume. Moreover, a significant negative correlation was observed between BNP and either LVEF and RVEF ($r = -0.52$, $p = 0.013$ and $r = -0.57$, $p = 0.005$, respectively). Conversely, ANP showed a significant correlation only with right atrium longitudinal diameter ($r = 0.48$, $p = 0.033$). Left ventricular ejection fraction (LVEF) was $23.7 \pm 1.6\%$, while right ventricular ejection fraction was $29.5 \pm 1.9\%$. End diastolic volumes were 268 ± 18 and 125 ± 10 ml for the left and right ventricle, respectively. BNP plasma values ranged from 54 to 783 with a mean value of 241 ± 42 pg/ml, ANP from 36 to 534, mean 134 ± 28 pg/ml. BNP positively correlated with either end-diastolic or end-systolic right ventricular volume, ($r = 0.61$, $p = 0.004$ and $r = 0.74$, $p < 0.001$, respectively), but not with left ventricular volume. Moreover, a significant negative correlation was observed between BNP and either LVEF and RVEF ($r = -0.52$, $p = 0.013$ and $r = -0.57$, $p = 0.005$, respectively). Conversely, ANP showed a significant correlation only with right atrium longitudinal diameter ($r = 0.48$, $p = 0.033$). Left ventricular ejection fraction (LVEF) was $23.7 \pm 1.6\%$, while right ventricular ejection fraction was $29.5 \pm 1.9\%$. End diastolic volumes were 268 ± 18 and 125 ± 10 ml for the left and right ventricle, respectively. BNP plasma values ranged from 54 to 783 with a mean value of 241 ± 42 pg/ml, ANP from 36 to 534, mean 134 ± 28 pg/ml. BNP positively correlated with either end-diastolic or end-systolic right ventricular volume, ($r = 0.61$, $p = 0.004$ and $r = 0.74$, $p < 0.001$, respectively), but not with left ventricular volume. Moreover, a significant negative correlation was observed between BNP and either LVEF and RVEF ($r = -0.52$, $p = 0.013$ and $r = -0.57$, $p = 0.005$, respectively). Conversely, ANP showed a significant correlation only with right atrium longitudinal diameter ($r = 0.48$, $p = 0.033$).

Conclusions: Right heart overload appears the most critical mechanism in plasma elevation of ANP and BNP. The role of right ventricular dysfunction, associated with

volume overload, which is known to independently worsen prognosis, could contribute, inducing compensatory elevation of plasma BNP, to its established prognostic power in heart failure.

293. Protocol Development for Assessment of Coronary Arteries, Valves, and Myocardial Function in Under Thirty Minutes

Mary P. Watkins, RT(MR),¹ Todd A. Williams, RT, BS, (MR),¹ Katherine A. Lehr, RN, BSN,¹ Samuel A. Wickline, MD,¹ Shelton D. Caruthers, PhD.²
¹Cardiovascular MR Laboratories, Washington University School of Medicine, St. Louis, MO, USA,
²Cardiovascular MR Laboratories, Washington University and Philips Medical Systems, St. Louis, MO, USA.

Introduction: Clinical acceptance of cardiac MR (CMR) depends not only on technical performance, but also on issues of patient comfort, cooperation, safety and throughput. To assume a role as an efficient screening tool, the development and implementation of a “Quick CMR Screening” examination is mandatory. If the standard diagnostic information can be acquired within thirty minutes, CMR might offer an alternative to echocardiography for primary screening of basic myocardial function and anatomy, mitral and aortic stenosis and regurgitation, and coronary artery disease.

Purpose: The purpose of this study is to define and evaluate a “Quick CMR Screening” protocol that offers a non-invasive assessment of the coronary arteries, valves, and myocardial function to serve as an efficient screening exam.

Methods: To produce a “Quick CMR Screening” examination of diagnostic quality, multiple imaging procedures must be combined. Development of this screening tool was conducted on eight patients (average age of 57 years) imaged on a clinical 1.5T scanner (Philips NT Intera Release 8.1.3, Best, The Netherlands) with a five-element cardiac synergy coil. Queued scan geometry was input from real-time interactive scan planning procedures. The imaging sequences comprised a steady-state gradient echo (bFFE) technique with sensitivity encoding (SENSE). In the first procedure shown (A), real-time interactive bFFE was used for image surveys. Next, breath hold SENSE bFFE was used to acquire the functional cine images (B). The valve images then were obtained with breath hold, velocity-encoded imaging using SENSE TFE (C). The coronaries

were completed with a 3D SENSE bFFE sequence employing a respiratory navigator (**D**). (Fig. 1)

Procedure A: To begin, an initial one minute SENSE reference scan must be acquired for subsequent reconstruction of all SENSE cine images. The study is initiated with interactive planning for surveys and queuing of geometry for cine images. In the scan queue, an interactive sequence using balanced FFE is preloaded along with the SENSE bFFE cine and valve sequences, with geometry inherit parameter pre-set to HLA, LVOT, VLA, SA, AO Valve 1, AO Valve 2, MV Valve (± 15 mm from the valve) to be defined interactively. The interactive sequence is started and multiple transverse, coronal, and sagittal scout views are acquired for later coronary imaging. Next, a transverse image is selected that demonstrates the left ventricle and atrium so that the VLA view can be positioned. Two SA surveys are positioned from the VLA, one at the midventricular level and one at the basal level of the left ventricle. Next, the basal SA survey is used for placing the LVOT view. From the LVOT view, placement of slices for the Aortic Valve views is made. Then the HLA view is positioned from the midventricular SA survey. A true SA view and Mitral Valve view can be angled from the HLA.

During the interactive sequence, each of the specified views are obtained and the geometries are stored in the respective geometry parameter.

Procedure B: In the next procedure, the cine sequences for a functional exam begin as a series of breath holds. Single slice cine images with at least 25 heart phases are obtained of the horizontal long axis (HLA), left ventricular outflow tract (LVOT), and vertical long axis (VLA). Multiple slice cine images with at least 15 heart phases are obtained in the short axis (SA) of both ventricles. Typically, nine 12 mm slices (acquired 3 slices per breath hold) are enough to cover the entire ventricle. The average breath holds, dependent upon heart rate, averaged between 10–15 seconds.

Procedure C: Next, quantitative flow sequences for the Aortic Valve and Mitral Valve are initiated. For aortic valve flow data and valve sizing by the continuity equation approach, two slices are placed 1.5 cm from either side of the valve in the aortic and LV outflow tract regions. For Mitral Valve flow data, one slice is placed in the LV just distal to the valve leaflets. These images require approximately 20-second breath holds with a minimum of 18 phases, and are retrospectively gated to the vector ECG. Encoding velocities (VENC) are pre-set for 250 cm/sec on the aortic side, 200 cm/sec on the LV outflow tract side, and 150 cm/sec for mitral inflow. Adjustments in VENC are made as required if aliasing is noted (primarily in the aortic regions for aortic stenosis), and the affected images are re-acquired.

Procedure D: Finally, the coronary acquisition is planned using the transverse, coronal, and sagittal views with a 3D slab of 60 slices, 1.5 mm thickness, overcontiguous, in the transverse plane. The respiratory navigator is placed on the right diaphragm and a regional shimming volume is placed over the heart. The slices originate at the inferior wall of the LV and continue to the middle of the pulmonary artery. The sequence time is approximately 2–4 minutes dependent upon the patient's heart rate and respiratory navigator acceptance level. This method ensures adequate screening imaging of the right, left, and circumflex artery.

Results: The study was conducted without difficulty and was tolerated well by all eight patients. The shortest exam time was 19 minutes, the longest exam time was 27 minutes, and average exam time was 23 minutes. The planning of the exam with the interactive tool requires some practice to develop the skill necessary for a quick screening. Also, positioning of the valve slices will necessitate additional time to define accurate placement since it is necessary to have the patient breath hold during the valve positioning, but not during the functional positioning. A prior

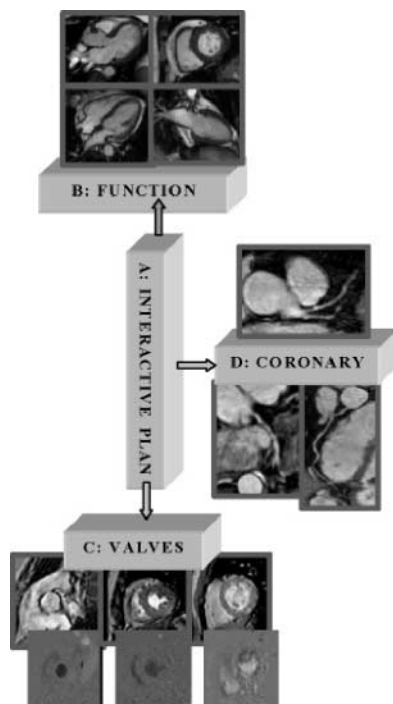


Figure 1. “Quick CMR Screening” protocol of myocardial function, valves, and coronary arteries.



Poster Abstracts: Clinical MRI—Non-ischemic Acquired Heart Disease

143

positioning of the coronary acquisition is not possible during the interactive sequence because of navigator and shim volume placement. In general, verbal comments from the patients indicated surprise at the speed of the exam.

Conclusions: The implementation of a comprehensive “Quick CMR Screening” protocol for evaluation of cardiovascular patients is possible in

under 30 minutes. The technical advances in interactive scan planning, improved imaging sequences that can be completed within a breath hold, and increased reconstruction speed have further advanced the ability for CMR imaging to serve as a high throughput diagnostic screening exam. CMR now provides a fast and non-invasive examination, conducive to patient comfort and rapid interpretation.